Materials Science & Engineering C 120 (2021) 111786

Contents lists available at ScienceDirect

Materials Science & Engineering C

journal homepage: www.elsevier.com/locate/msec

Selective delivery of silver nanoparticles for improved treatment of biofilm skin infection using bacteria-responsive microparticles loaded into dissolving microneedles

Andi Dian Permana [a,*], Qonita Kurnia Anjani [b], Sartini [c], Emilia Utomo [b], Fabiana Volpe-Zanutto [b,d], Alejandro J. Paredes [b], Yayu Mulsiani Evary [e], Sandra Aulia Mardikasari [a], Muh. Rezky Pratama [a], Irma Nurfadilah Tuany [a], Ryan F. Donnelly [b]

[a] Department of Pharmaceutics, Faculty of Pharmacy, Hasanuddin University, Makassar 90245, Indonesia
[b] School of Pharmacy, Queen's University Belfast, Belfast BT9 7BL, UK
[c] Department of Pharmaceutical Microbiology, Faculty of Pharmacy, Hasanuddin University, Makassar 90245, Indonesia
[d] Faculty of Pharmaceutical Sciences, University of Campinas, R. Cândido Portinari, 200 - Cidade Universitária, Campinas, SP 13083-871, Brazil
[e] Department of Phytochemistry, Faculty of Pharmacy, Hasanuddin University, Makassar 90245, Indonesia

ARTICLE INFO

Keywords:
Silver nanoparticles
Responsive microparticles
Wound
Biofilm
Microneedles
Staphylococcus aureus
Pseudomonas aeruginosa

ABSTRACT

The treatment of infected chronic wounds has been hampered by development of bacterial biofilms and the low penetration of antibacterial compounds delivered by conventional dosage forms. Numerous bacterial biofilm formers have shown resistance to synthetic antibacterial agents. In this study, we explore the potential of silver nanoparticles (NPs) synthesized using green tea extract as antibiofilm agents against *Staphylococcus aureus* (SA) and *Pseudomonas aeruginosa* (PA) biofilms. Due to the toxicity of silver NPs, for the first time, silver NPs were incorporated into bacteria-responsive microparticles (MPs) prepared from poly (Ɛ-caprolactone) decorated with chitosan. The *in vitro* release of silver NPs from MPs increased up to 9-times in the presence of SA and PA, showing the selectivity of this approach. Incorporation of the MPs into dissolving microneedles (DMNs) could enhance the dermatokinetic profiles of silver NPs compared to DMNs containing silver NPs without MP formulations and conventional cream formulations. Furthermore, 100% of bacterial bioburdens were eradicated on *ex vivo* biofilm model in rat skin following 60 h of the administration of this system. The findings revealed here confirmed the feasibility of the loading of silver NPs into responsive MPs for improved antibiofilm activities when delivered using DMNs. Following on from these promising results, toxicity and *in vivo* pharmacodynamic studies should now be carried out in an appropriate model.

1. Introduction

The management of burns and chronic wounds is hampered by several clinical complications, resulting in difficulty in healing and the requirement of prolonged therapy [1–3]. In an attempt to overcome this health issue, about $50 billion have been spent annually on chronic wounds therapy [4]. Surgical debridement, including removal of necrotic and infected tissue has become the main option for the wound managements. Antimicrobial agents systemically and/or topically have also been utilized for wound treatment. However, prolonged use of antimicrobial agents could potentially lead to undesired systemic adverse effects [5,6]. Moreover, more than 80% of chronic wounds in humans involve bacterial biofilm formation [7]. Although it has been reported that biofilms are able to be formed by several bacteria, the most commonly bacteria found are *Staphylococcus aureus* (SA) and *Pseudomonas aeruginosa* (PA) [8,9].

Bacterial biofilms are formed by immobile bacteria surrounded inside a protective environment, consisting of polysaccharides, nucleic acids, extracellular DNA, proteins, and lipids, therefore established a compact structure of hydrated extracellular polymeric substances (EPS). The presence of EPS in a biofilm limits the penetration of antimicrobial therapeutics into biofilms. Accordingly, the wound treatment using conventional antibiotic is frequently ineffective [10,11]. Biofilms are, therefore, a significant obstacle to wound healing [7]. To sterilize the

* Corresponding author at: Faculty of Pharmacy, Hasanuddin University, Indonesia.
E-mail address: andi.dian.permana@farmasi.unhas.ac.id (A.D. Permana).

https://doi.org/10.1016/j.msec.2020.111786
Received 15 October 2020; Received in revised form 21 November 2020; Accepted 4 December 2020
Available online 10 December 2020

wound, existing process of biofilm removal employs bleach or other erosive agents [12], causing poor compliance of patients and excessive health care management [13]. As previously stated, surgical debridement of infected wounds is able to remove biofilm formed in the wound. However, 2 days after removal, the biofilms are found to be formed again [14]. To overcome this, long-term antibiotic use has been employed. Unfortunately, this can lead to development of antibiotic-resistant bacteria [15]. As a result, a new drug delivery system which is potentially able to disturb and destroy the bacteria forming biofilms is required as an alternative management strategy for treatment of chronic wound.

Metal nanoparticles (NPs), particularly silver NPs, have shown excellent antibacterial and antibiofilm activities against several bacterial pathogens, including SA and PA [16,17]. There are numerous studies on the green synthesis and antimicrobial activity of silver NPs [18,19]. Several methods have been developed to prepare silver NPs. Among them, the application of a natural compound from plant extracts as a reducing agent for silver NPs has been preferred because it is eco-friendly, simple, fast and cheap [20,21]. Green tea (*Camellia sinensis*) is a natural product that has been reported to possess high content of polyphenolic compounds. Importantly, it has been extensively used in silver NPs synthesis [22]. Generally, green tea contains epigallocatechin-3-gallate (EGCG), epigallocatechin, epicatechin-3-gallate and epicatechin [23], which have capacity as reducing and capping compounds in silver NPs synthesis [23]. Despite the effectiveness of silver NPs, it has been reported that silver NPs could potentially result in toxicity to human cells [24,25]. Therefore, it is required to develop a selective drug delivery system which can avoid the exposure of silver NPs to non-desired site.

Our previous study has shown that incorporation of doxycycline into poly (Ɛ-caprolactone) (PCL) NPs decorated with chitosan has successfully delivered doxycycline into infection sites without being degraded in normal tissue in *ex vivo* studies [26]. Lipolytic esterase produced by SA and PA has been found to initiate the biocatalytic hydrolysis of poly (Ɛ-caprolactone) (PCL) in nanogel formulations [27]. Moreover, while the surface of chitosan NPs are positive, the biofilm EPS and bacterial cell walls possess negative charges. Therefore, chitosan is likely to demonstrate a high attraction to infected sites [28]. Considering these characteristics, these polymers can be used as appropriate materials to specifically deliver antimicrobial compounds to the infected tissues only. Therefore, this approach could potentially avoid the exposure to healthy tissues, resulting in a safe therapy approach. Moreover, to further localize the particles in the skin, microparticles (MPs) have been considered to show higher drug retentions compared to NPs [29]. Accordingly, the formulation of silver NPs into PCL MPs decorated with chitosan could potentially improve the effectiveness of biofilm targeting in skin wound infections.

It must be considered that to deliver the antimicrobial agents to the infected area, the dense physical obstacle presented by biofilms, must be overcome. Antimicrobial agents administered systemically are not able to effectively reach the infected areas [30]. In addition to the presence of biofilms, in infected wounds, the necrotic tissue covering the wound bed is another issue to consider in the treatment process [31]. Antimicrobial agents delivered from conventional topical dosage forms, including dressings, creams and gels, have been found to display poor penetration due to this obstruction, leading to low concentrations of the antimicrobial agents in the infected area [32,33]. Although it has been reported that silver NPs can penetrate both damaged or intact human skin [23], the incorporation into MPs could potentially decrease the skin penetration ability. Accordingly, a suitable device which can improve the penetrability of silver nanoparticles-loaded microparticles through the biofilm and the necrotic tissue is necessary, as this would circumvent the requirement of the removal of necrotic tissue. Dissolving microneedles (DMNs) can by-pass the major skin barrier [34], and, is able to penetrate the necrotic tissue and biofilms in the infected skins [26,31]. Importantly, a localized, painless, rapid delivery and patient-compliant are the significant advantages of DMNs administration [35]. DMNs are made from biocompatible and biodegradable polymers, they are self-dissolvable and their utilization does not generate any biohazardous sharps waste [36]. Bearing in mind the potential benefits of this approach, the incorporation of MPs laden with silver NPs into DMNs could potentially increase the amount of silver NPs penetrating the biofilm and necrotic tissue of infected skin and, therefore, could hypothetically improve the management of burns and chronic wounds.

Herein, we present, for the first time, the development of MPs decorated with chitosan laden with silver NPs produced from green tea extract, incorporated into DMNs as an innovative delivery system for prospective enhanced management of chronic wounds with the presence of bacterial biofilms. Silver NPs were evaluated for their size, zeta potential, polydispersity index, UV spectra, shape, FTIR, XRD, antibacterial activities and antibiofilm activities against SA and PA. Furthermore, in the MPs formulation, PCL was selected as the responsive polymer matrix, and decorated with chitosan to create positively charged MPs. Importantly, the release profiles of silver NPs from MPs were determined with and without the presence of SA and PA. The MPs were further incorporated into DMNs, which were characterized for their mechanical and insertion properties. *Ex vivo* dermatokinetic profiles of silver NPs were investigated in normal porcine skin and in an *ex vivo* biofilm model in excised rat skin. Finally, to assess the potential efficacy of this innovative approach, the capability to penetrate and eradicate the bacterial biofilms were carried out in *ex vivo* skin biofilm model.

2. Materials and methods

2.1. Materials

Silver nitrate ($AgNO_3$) was purchased from Merck KGaA (Darmstadt, Germany). Dichloromethane (DCM), poly (vinyl alcohol) (PVA) (9–10 kDa), poly (Ɛ-caprolactone) (PCL) (45 kDa) and chitosan were obtained from Sigma-Aldrich (Dorset, UK). Poly(vinylpyrrolidone) PVP (58 kDa) was provided by Ashland (Kidderminster, UK). All other reagents were of analytical grade and purchased from standard commercial suppliers.

2.2. Synthesis silver NPs using green tea extract

Silver NPs were synthesized through biological reduction of $AgNO_3$ using green tea extract [23]. Green tea extract was obtained from our previous study [37]. Briefly, coarse powder of green tea was extracted with water (1:10 ratio of green tea:water) using a high-pressured extraction (PT. IFI, Makassar, Indonesia) with a pressure of 700 Bar. The resultant water extract was then lyophilized using a freeze drier (Lyovac GT2, GEA, Düsseldorf, Germany) to obtain the dried extracts.

Initially, the stock solution of tea extract was prepared at the concentration of 1% w/v in distilled water and 0.1 mM of $AgNO_3$ was prepared in distilled water. To prepare silver NPs, $AgNO_3$ solution was added to green tea extract solution and the mixture was stirred at 200 rpm at 25 °C. The proportions of $AgNO_3$ solution and green tea extract solution were varied at 1:1, 1:2, 1:4 and 1:8 to synthesize of silver NPs. Furthermore, in order to optimize the synthesis duration, different reaction times were evaluated as follows: 0.5 h, 1 h, 2 h, 3 h, 4 h, 5 h and 6 h. Silver NPs were collected by centrifugation for 60 min at 14,000 rpm. The precipitated NPs were washed three times with distilled water. To produce the uniform dispersion for the further studies, after final centrifugation, 1 mL of distilled water was added to each 0.5 g of precipitated silver NPs.

2.3. Characterization of silver NPs

The formation of silver NPs was observed by using UV–vis spectrophotometer (Model UV-2500, Shimadzu Co., Ltd., Tokyo, Japan). The scanning was performed between 200 and 800 nm. Additionally, the absorbance of silver NPs at 410 nm was determined to further

investigate the successful formation of silver NPs.

The diameter, polydispersity index (PDI) and zeta potential of silver NPs were determined using the Zetasizer Nano ZS (Malvern Instruments Co, UK). The determinations were carried at 25 °C using a fixed angle of 173°. To visualize the morphology of silver NPs, scanning electron microscope (SEM) (JEM-1400Plus; JEOL, Tokyo, Japan) was used.

A Fourier transform infrared (FTIR) spectrometer (Accutrac FT/IR-4100™ Series, Perkin Elmer, USA) was used to investigate the functional groups involved in the synthesis of silver NPs. Additionally, X-ray powder diffraction of silver NPs was observed using an X-ray diffractometer (Rigaku Corporation, Kent, England).

2.4. In vitro antibacterial activities

2.4.1. Culture of bacterial strains

Staphylococcus aureus (ATCC® 25923) (SA) and *Pseudomonas aeruginosa* (ATCC® 9027) (PA) were used in this study and were obtained from Thermo Fisher Scientific, Waltham, MA, USA. The bacterial cultures were preserved at 4 °C and sub-cultured on fresh media at routine interval times. Before every antibacterial experiment, the bacterial cultures were grown in tryptic soy broth (TSB) 37 °C overnight. After cultivation, the bacterial suspensions were centrifuged at 3000 rpm for 25 min to obtain the pellet. The pellet obtained was suspended in fresh TSB and optical density of bacterial suspension was set at 550 nm to attain an equal to 1.5×10^8 CFU/mL.

2.4.2. Determination of minimum inhibitory concentration and minimum bactericidal concentration

The protocol of the Clinical and Laboratory Standards Institute was applied to determine the minimal inhibitory concentrations (MIC) and minimal bactericidal concentrations (MBC) of silver NPs [38]. This study was carried out using a microtiter broth dilution technique in 96-well bottom-plate. Initially, 100 μL of silver NPs with different concentrations were mixed with 100 μL bacteria suspension (1.5×10^8 CFU/mL) in a 96-well plate in their respective medium to achieve in 2×10^5 CFU/mL of bacteria. The mixtures were incubated for 24 h at 37 °C. For MIC determination, each plate was observed, and the MIC was expressed as the lowest concentration of silver NPs showing no visible growth of the bacterial. To determine MBC, 10 μL from wells containing silver NPs with the concentrations at MIC values and all concentrations above the MIC values were cultivated to TSA plates and were incubated at 37 °C for 24 h. The number of bacterial colonies growing was totaled. Finally, the MBC was expressed as the smallest silver NPs concentration that eradicated 99.9% of the bacterial growth.

2.4.3. Time kill assay

Time-killing kinetics of silver NPs against SA and PA were investigated according to the technique published previously [26,39,40]. Briefly, the bacterial suspensions were mixed with different concentrations of silver NPs corresponding to MIC, 2 × MICs and 4 × MICs to achieve 2×10^5 CFU/mL of bacteria. These mixtures were incubated at 37 °C. At predefined time intervals, aliquots of 20 μL from the cultures were taken and cultivated aseptically to TSA plates media. The TSA plates were further incubated for 24h at 37 °C and the number of bacterial colonies growing were counted, expressed as colony forming unit (CFU/mL). Finally, a curve of the log CFU/mL *versus* time-kill was constructed.

2.5. In vitro antibiofilm activities

2.5.1. 96-well microtiter plate (MTP) biofilm study

The crystal violet method was applied to investigate the *in vitro* antibiofilm activity of silver NPs against biofilm-grown SA and PA [41]. Initially, the bacterial cultures were grown in TSB enriched with NaCl (3% w/v) and glucose (0.5% w/v) (TSB-NG) and were diluted to attain 2×10^5 CFU/mL of bacteria. To create preformed biofilms, 200 μL of the bacterial suspensions were incubated at 37 °C for 24 h in a 96-well plate. Subsequently, the liquid media containing non-adherent cells was removed from the wells. The wells were cautiously washed with sterile PBS three times in order to detach any non-adherent bacteria and the biofilms were observed to be attached in the wells. Aliquots of 200 μL of silver NPs with the concentrations corresponding to MIC, 2 × MICs and 4 × MICs of silver NPs were then added to the preformed biofilms. TSB-NG was added as control and the microplates were incubated at 37 °C for 24 h. Afterwards, the non-adherent bacterial cells were detached from the wells. The remaining biofilms in the wells were washed with 200 μL of sterile PBS three times. The microplates were left for 1 h at 25 °C to dry. Following this, 200 μL of crystal violet (1% w/v) was added to stain the persisted biofilms in the wells. The plates were incubated at room temperature for 15 min. The wells were rinsed with sterile distilled water three times to remove free crystal violet. To dissolve the crystal violets absorbed by bacterial cells, 200 μL of ethanol was added into each well. The absorbance of ethanol solutions containing absorbed crystal violet, presenting the amount of biofilm, was measured at 595 nm using UV–vis spectrophotometer. Finally, to calculate the killing percentage of silver NPs, Eq. (1) was used.

$$\text{Killing percentage} = \frac{Abs_{control} - Abs_{experimental}}{Abs_{control}} \times 100\% \quad (1)$$

2.5.2. Colony biofilm model (CBM)

The antibiofilm activities of silver NPs were also studied in the CBM [2], with minor changes. Initially, sterile 10 mm poly(carbonate) discs were located on the TSA media plates in Petri dishes and 50 μL of the diluted bacterial with colony counted of 2×10^5 CFU/mL were added onto the discs. To allow the formation of biofilm, the dishes were incubated at 37 °C for 72 h. Every 4 days, the discs were placed to fresh TSA plates. Following this, 100 μL of silver NPs with the concentrations equivalent to MIC, 2 × MICs and 4 × MICs were added into the biofilm formed on the surface of the discs. The Petri dishes were further placed in an incubator for 24 h at 37 °C. After incubation, 5 mL of TSB was mixed with each disc in a tube. The tube was vortexed for 5 min to disturb the biofilms and to detach the bacteria from the discs. The bacterial suspensions were subsequently diluted and 20 μL of bacterial suspensions were cultured into TSA plates. The dishes were placed in the incubator for 24 h at 37 °C and the viable CFU were observed. The biofilms growing on the discs without any treatments were utilized as controls. Finally, to determine the killing percentage, Eq. (2) was applied.

$$\text{Killing percentage} = \frac{CFU_{control} - CFU_{experimental}}{CFU_{control}} \times 100\% \quad (2)$$

2.6. Formulation of PCL MPs loaded with silver NPs

Microparticles (MPs) containing silver NPs were prepared using a solvent/non-solvent technique [42], with minor modification. The composition of each formulation is depicted in Table 1. Initially, PCL was dissolved in acetone and silver NPs were dispersed in water. Both solutions were then homogenized using an Ultra Turrax homogenizer (IKA, model T25, impeller 10 G, Germany) at 5000 rpm for 30 min. The mixture was further precipitated using ethanol containing PVP by continuing the homogenization process for 30 min. In order to evaporate the organic phase, the MPs were stirred at room temperature for 6 h. The

Table 1
Formula of silver NPs-loaded MPs.

	MP1	MP2	MP3	MP4	MP5
PCL (g/5 ml DCM)	0.75	1	1.25	1.5	1.75
Silver NPs dispersion (mL)	1	1	1	1	1
Chitosan (g/5 mL)	1	1	1	1	1
PVP 2% (mL)	10	10	10	10	10

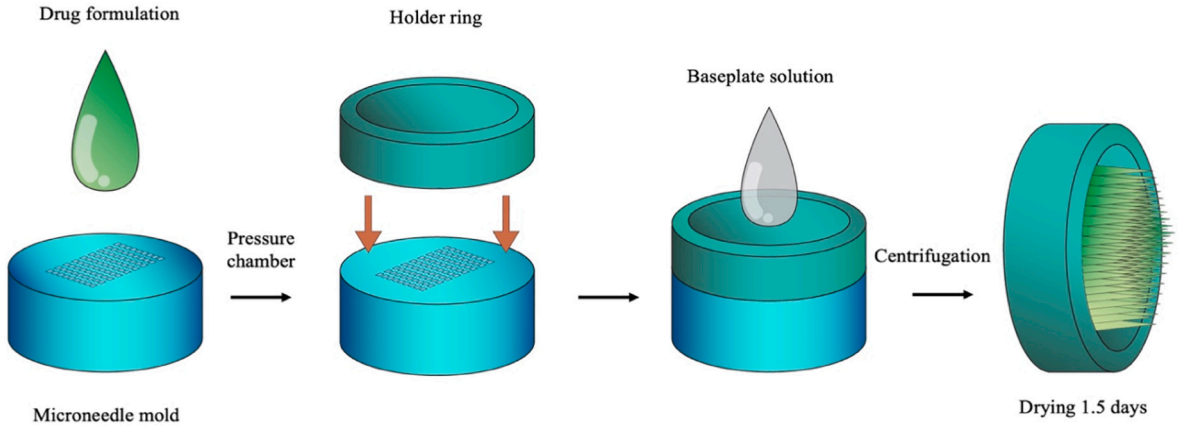

Fig. 1. Schematic of DMNs preparation.

formed MPs were washed three times with distilled water by centrifugation at 3000 rpm for 30 min. After the final washing, the pellets were dispersed in 5 mL of chitosan solution (in 0.5% v/v acetic acid) [26]. The dispersions were stirred for 2 h to form MPs-coated with chitosan. The coated MPs were washed using the same protocol.

2.7. Characterization of PCL MPs

The particle sizes and size distribution were determined using a Mastersizer 2000 size analyzer (Malvern Instruments, Malvern, UK). The size distribution was presented as SPAN value. The zeta potential was determined using a Zetasizer Nano ZS (Malvern Instruments, Malvern, UK).

The efficiency of encapsulation (EE) of silver NPs in MP formulations was determined using an indirect method. After the first centrifugation in the washing process, the supernatant was collected and the amount of unencapsulated silver NPs was quantified using atomic absorption spectroscopy (AAS) (Varian SpectrAA-300 AAS). It is important to note that the washing centrifugation did not precipitate the silver NPs. The EE was calculated using Eq. (3).

$$\text{EE}\ (\%) = \frac{\textit{Silver NPs total} - \textit{Silver NPs free}}{\textit{Silver NPs total}} \times 100\% \quad (3)$$

The determination of loading capacity (LC) of silver NPs in MP formulations was performed by initially drying the washed MPs in the oven for 24 h at 37 °C, forming dry MPs. Following this, 10 mg of dry MPs was suspended in 10 mL of distilled water. Afterwards, 10 mL of acetone was added into the dispersion and sonicated for 2 h in a bath sonicator. The mixtures were finally centrifuged at 3000 rpm for 15 min and the supernatant collected was analyzed using AAS. The DL was calculated using Eq. (4).

$$\text{LC}\ (\%) = \frac{\textit{Amount of encapsulated silver NPs}}{\textit{Total weight}} \times 100\% \quad (4)$$

The morphologies of the silver NPs loaded with MPs were observed using a scanning electron microscope (SEM).

2.8. In vitro release study of silver NPs from MPs in bacterial cultures

To evaluate the selectivity of the release profile of silver NPs from MPs, the studies were conducted with or without the bacterial cultures [27]. In brief, MPs corresponding to 5 mg of silver NPs were dispersed in 10 mL of release media. For the release media containing bacterial cultures, the optical density of cultures was set to 0.1 at 550 nm. The release study was carried out in an orbital shaker at 37 °C at 100 rpm. Aliquots of 0.5 mL of sample were taken at predetermined time intervals and the amount of silver NPs release was finally quantified using AAS.

2.9. Fabrication of two-layered dissolving MNs

Two-layered DMNs containing silver NPs loaded MPs were prepared using silicone moulds by a two-step casting technique [40]. The moulds used in this study had needle density of 16 × 16, height of needles of 850 μm [600 μm pyramidal tip, 250 μm base column] and 300 μm width at base and 300 μm interspacing. Five different formulations were prepared using an aqueous blend comprised of 20% w/w of PVA (9–10 kDa) and 20% w/w of PVP (58 kDa), namely F1 (10% w/w of dry MPs: 90% w/w of MN matrix), F2 (20% w/w of dry MPs: 80% w/w of MN matrix), F3 (30% w/w of dry MPs: 70% w/w of MN matrix), F4 (40% w/w of dry MPs: 60% w/w of MN matrix) and F5 (50% w/w of dry MPs: 60% w/w of MN matrix). To prepare the first layer of DMNs, an excess amount of each formulation was dispensed onto the moulds and placed in a positive pressure chamber with pressure of 5 bar for 2 min. Following this, a spatula was used to remove the excess formulation on the moulds. The formulations were placed at room temperature for 6 h. The second layer was prepared from an aqueous blend of PVP (90 kDa) 30% w/w and glycerol 1.5% w/w. The aqueous gel was poured onto the first layer formulation with the application of a silicone ring with external diameter of 23 mm, internal diameter of 18 mm, thickness of 3 mm connected to the MN moulds. Subsequently, the two-layered DMNs in the moulds were centrifuged for 15 min at 3500 rpm. Finally, the DMNs were again placed at room temperature for 48 h and at 37 °C for 12 h. DMNs containing silver NPs without MP formulation were also prepared using the same procedure. The DMNs were visually observed using a Leica EZ4D light microscope (Leica Microscope, Milton Keynes, UK) and scanning electron microscope (SEM) TM3030 (Hitachi, Krefeld, Germany). Fig. 1 shows schematic of DMNs preparation.

2.10. Evaluation of mechanical and insertion properties of dissolving MNs

To evaluate the performance of DMNs, several characterizations were performed. A TA-TX2 Texture Analyzer (Stable Microsystem, Haslmere, UK) was applied to investigate the mechanical strength of DMNs, as described in our previous study [43]. Importantly, Parafilm®M as a validated artificial skin-simulant was used to evaluate the insertion ability of the DMNs, as previously described [44]. In addition, an optical coherence tomography (OCT) microscope (Michelson Diagnostics Ltd., Kent, UK) was also applied to observe the insertion depth of selected DMN formulations in Parafilm® M and full-thickness porcine skin.

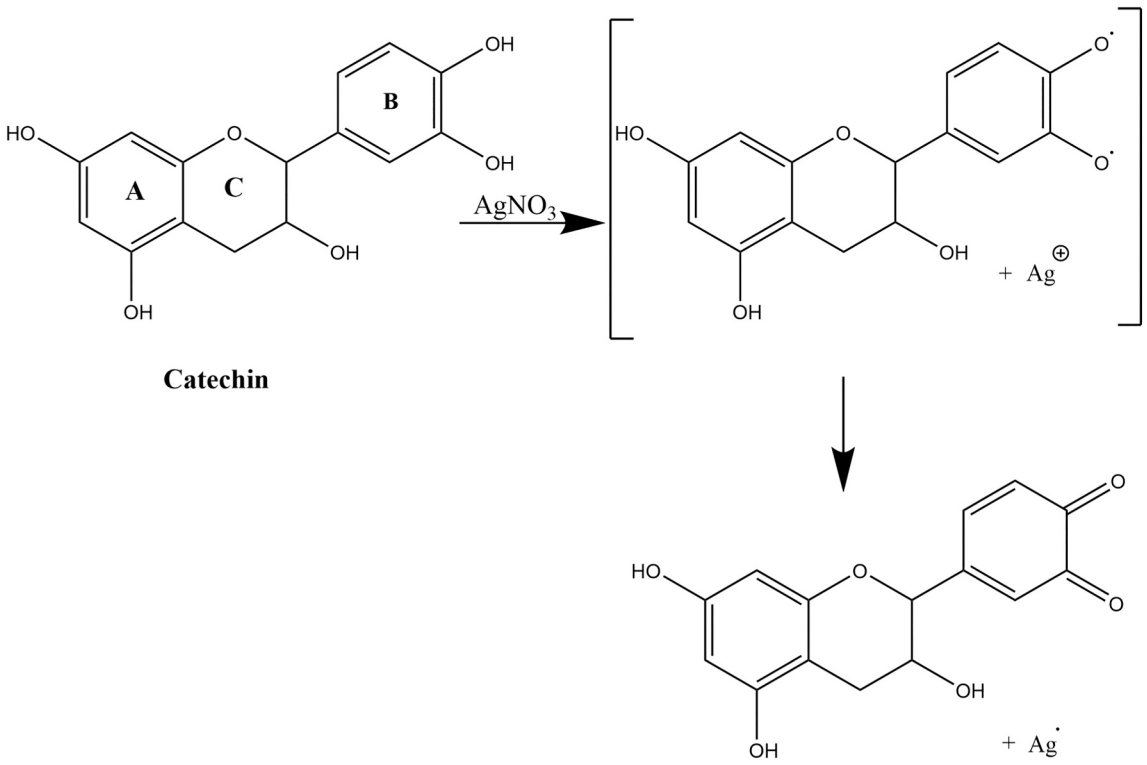

Fig. 2. Schematic representation of Ag^{+} reduction by the polyphenol compound in green tea (cathechin), resulting in the formation of silver NPs. (For interpretation of the references to color in this figure legend, the reader is referred to the web version of this article.)

2.11. Dissolution study, ex vivo dermatokinetic studies and antibiofilm activity in ex vivo model of biofilm on rat skin

2.11.1. Preparation of ex vivo model of biofilm on rat skin

Abdominal skins of Wistar rat were shaved and equilibrated in PBS (pH 7.4) prior to the experiment. The rat skins were decontaminated in 70% ethanol for 1 h. Prior to the use, the skins were placed in a biosafety cabinet for 20 min to evaporate the ethanol. In brief, wound was created in the surface of the skin using biopsy punch (Stiefel, Middlesex, UK). Following this, *ex vivo* models of biofilm on rat skin were generated using the procedures described earlier [2], with minor modifications. The skins were p laced on TSA plates and 50 μL of the diluted bacterial suspensions 2×10^5 CFU/mL were dropped to the wound of the skin and spread homogeneously. To allow the formation of the biofilm on the wounded skin, the plates were incubated at 37 °C with the skins were moved to new TSA plates every day for 5 days.

2.11.2. Ex vivo dermatokinetic studies

Ex vivo dermatokinetic studies of DMNs containing silver NPs and silver NPS loaded MPs were performed in normal skins and *ex vivo* biofilm model in rat skins, using the method described in our previous studies [34,36]. Briefly, the DMNs were manually inserted for 30 s into the skins which were previously attached to the donor compartment of the Franz cell diffusion cells. The donor compartment was further attached to the receiver compartment filled with PBS (pH 7.4). To avoid the movement of DMNs during the study, 5 g of mass made from stainless-steel was employed on top of the DMNs. The study was carried out at 37 ± 1 °C at 600 rpm. To evaluate the amount of silver NPs in the skins at different predetermined time intervals, the DMNs were detached from the skins. The skins were washed three times, placed into glass vials and 2.5 mL water was added into the skins. The mixtures were vortexed for 30 min and centrifuged at 3000 rpm for 15 min. The amount of silver in the supernatant was quantified using AAS. The dermatokinetic profiles were calculated using PKSolver (China Pharmaceutical University, Nanjing, China) [45].

2.11.3. Antibiofilm activity in ex vivo model of biofilm on rat skins

Ex vivo antibiofilm activities of DMNs containing silver NPs and silver NPS loaded MPs were studied using the technique published previously [2,46], with minor modifications. To investigate the antibiofilm activity of DMNs, the supernatants obtained from dermatokinetic studies (20 μL) following 12 h, 24 h, 48 h and 60 h application time were taken and dropped into TSA plates. The plates were placed in a 37 °C incubator for 24 h. In addition, as a comparison, the conventional creams containing silver NPs and silver NPs loaded MPs were prepared and evaluated for their *ex vivo* antibiofilm activities using the same method. Infected skins without any treatments were employed as a positive control. The numbers of viable CFU were finally calculated.

2.12. Statistical analysis

All data in this study were presented as means ± standard deviation (SD) of the mean and were calculated using Microsoft Excel® 2016 (Microsoft Corporation, Redmond, USA). GraphPad Prism® version 6 (GraphPad Software, San Diego, California, USA) was used to statistically analyzed the data. A value $p < 0.05$ was noted as a statistical significance.

3. Results and discussion

3.1. Synthesis and characterization of silver NPs using green tea extract

In this study, silver NPs were prepared and synthesized using a biogenic way. In this method, the use of plant extract offers numerous benefits compared to other synthesis methods, including low-cost, simplicity, and, importantly, this method does not use of organic solvents and hazardous materials [23,47]. Among several plants that can be used in the biogenic synthesis of silver NPs, green tea (*Camellia sinensis*) was selected due to its rich content of polyphenolic compounds (mainly catechin), which act as reducing and capping agents [23]. During the synthesis process, the interaction of $AgNO_3$ with the green

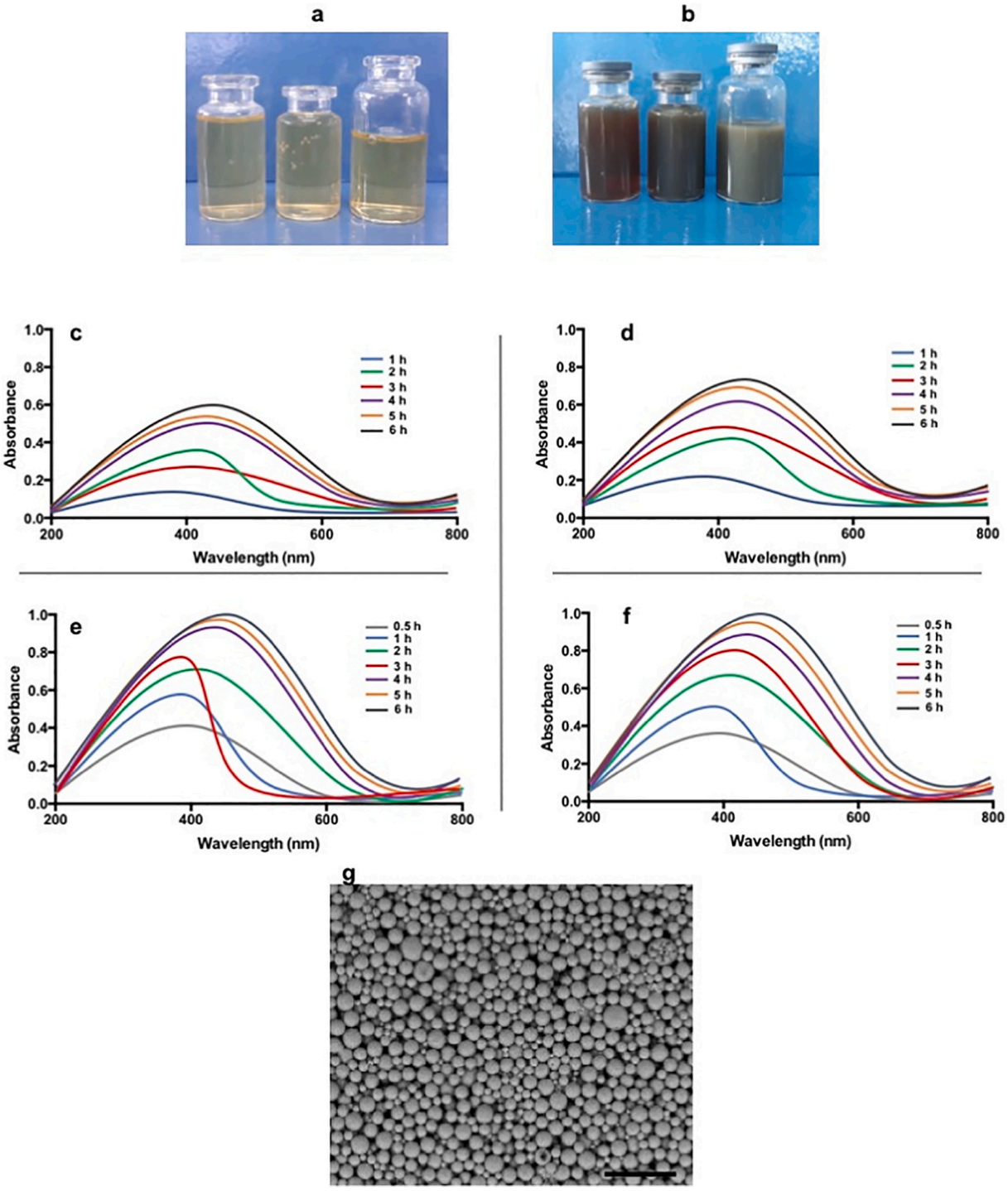

Fig. 3. The green tea extract solution (**a**) and the formation of silver NPs, indicated by the suspension changing to a dark color (**b**). UV–Vis spectra of the silver NPs synthesized with the ratio of $AgNO_3$ solution and green tea extract solution at 1:1 (**c**) 1:2 (**d**) 1:4 (**e**) and 1:8 (**f**) with different synthesis times. SEM images of selected silver NPs at a magnification power of 30,000×. (The black scale bar represents a length of 200 nm) (**g**). (For interpretation of the references to color in this figure legend, the reader is referred to the web version of this article.)

tea extract led to the reduction of Ag^+ to Ag. The predicted mechanism of reduction of Ag^+ by the green tea polyphenols is depicted in Fig. 2. Based on present result, a possible mechanism was proposed to the reduction of Ag^+ ions with catechin, the main compound of green tea extract. Fig. 2 shows first a nucleation reaction, representing the reduction of Ag^+ ions into metallic Ag° with –OH ring B present in the catechin structure [48]. The formation of the silver NPs was implied by the suspension changing color to dark color [22,49], as shown in Fig. 3a and b.

The silver NPs formation was confirmed using UV–vis spectroscopy. This spectroscopy is able to detect the surface plasmon resonance (SPR) absorption band at 410 nm in the UV–vis region [50]. The SPR formation occurred on the surface of the silver NPs, induced by the resonant oscillation of conducting electrons present which was produced from an interaction with electromagnetic waves [23,50]. In this study, two optimizations were performed, namely the ratio of $AgNO_3$ solution and

Table 2
The absorption of the silver NPs synthesized with the various ratio of $AgNO_3$ solution and green tea extract solution at 410 nm (means ± SD, $n = 3$).

Ratio $AgNO_3$ and extract	Synthesis time						
	0. 5 h	1 h	2 h	3 h	4 h	5 h	6 h
1:1	0	0.13 ± 0.02	0.27 ± 0.03	0.37 ± 0.04	0.52 ± 0.08	0.54 ± 0.07	0.56 ± 0.06
1:2	0	0.16 ± 0.02	0.27 ± 0.03	0.41 ± 0.04	0.58 ± 0.09	0.61 ± 0.09	0.62 ± 0.08
1:4	0.35 ± 0.04	0.45 ± 0.07	0.66 ± 0.08	0.77 ± 0.09	0.91 ± 0.09	0.94 ± 0.08	0.95 ± 0.07
1:8	0.39 ± 0.06	0.48 ± 0.05	0.71 ± 0.09	0.80 ± 0.10	0.97 ± 0.20	0.98 ± 0.09	0.98 ± 0.10

green tea extract solution, as well as the synthesis time. Fig. 3c-f show the UV–Vis absorption spectrums of silver NPs prepared from the different treatment process.

The increases on the green tea extract concentration and the synthesis time led to an improved formation of silver NPs, indicated by the high absorption in UV–Vis spectra. To further investigate the effect of the green tea extract solution and the synthesis time, the absorptions of silver NPs at 410 nm were determined, as shown in Table 2. It was found that the absorptions of silver NPs prepared from the ratios 1:4 and 1:8 were significantly higher ($p < 0.05$) than other ratios. Moreover, several studies have shown that the increase of reducing agents concentration and synthesis time could potentially affect the formation of silver NPs [23,51,52]. Accordingly, these ratios were selected for further.

The mean hydrodynamic sizes of silver NPs were in the range of 28.76 ± 3.12 nm–35.71 ± 5.23 nm with the mean PDI of between 0.21 ± 0.01 and 0.26 ± 0.02. SEM images of silver NPs shoed that the size obtained was around 30 nm (Fig. 1g). The zeta potentials were found to be in the range of −33.4 ± 3.18 mV to −38.1 ± 3.13 mV. Our results were similar to the characteristics of silver NPs reported by Rolim et al., showing that the silver NPs showed the average hydrodynamic size of 34.68 ± 4.95 nm, the average PDI of 0.28 ± 0.01 and the average zeta potential of - 35.5 ± 3.32 mV [23]. In this study, the negative zeta potentials were obtained due to the presence of polyphenol contained in the green tea, showing the negative charge [53].

FTIR spectroscopy study was performed to identify the functional groups of chemical composition of the silver NPs surface. The FTIR spectra of green tea extract and silver NPs are depicted in Fig. 4a. The strong signals were observed in both spectra at 3400–3350 cm^{-1}, 2930–2925 cm^{-1}, 1380–1360 cm^{-1}, and 1050–1040 cm^{-1} due to N—H stretching (amides), C—H stretching (alkanes), hydroxyl groups (phenolic hydroxyl) and C-stretching (ether groups). Furthermore, other peaks at 919 cm^{-1}, 1239 cm^{-1}, 1460 cm^{-1} and 1705 cm^{-1} were observed in silver NPs, attributed to alkene groups (C—H stretching) alkene groups (C═C stretching), aliphatic amines (C—N stretching vibrations), and tertiary ammonium ions, polyphenols, aliphatic amines (C—N stretching vibrations), respectively. This study implied that several compounds, namely amides, carboxyl, amino groups and polyphenols from green tea, could involve in the synthesis of silver NPs. It has been reported that polyphenols, protein, and amino acid are the main compounds in green tea [23]. These compounds, mainly polyphenols, could play important role in the reduction of $AgNO_3$ and the stabilization of silver NPs [54]. The XRD diffractogram of silver NPs is presented in Fig. 4b. The result depicted that silver NPs exhibited sharp characteristics peaks at 38.19°, 45.97°, 63.98°, and 78.02° due to the (111), (200), (220), and (311) of faced center cubic (FCC) planes lattice of metallic silver [23,55]. The sharp peak at 38.19° could be due to the

Table 3
MIC and MBC values of the silver NPs synthesized with different ratio of $AgNO_3$ solution and green tea extract solution ($n = 3$).

Ratio of $AgNO_3$ and extract	MIC values (μg/mL) of silver NPs in different synthesis time against SA						
	0.5 h	1 h	2 h	3 h	4 h	5 h	6 h
1:4	5	5	2.5	2.5	1.25	1.25	1.25
1:8	5	5	2.5	2.5	1.25	1.25	1.25
MIC values (μg/mL) of silver NPs in different synthesis time against PA							
1:4	10	10	5	5	2.5	2.5	2.5
1:8	10	10	5	5	2.5	2.5	2.5
MBC values (μg/mL) of silver NPs in different synthesis time against SA							
1:4	10	10	5	5	2.5	2.5	2.5
1:8	10	10	5	5	2.5	2.5	2.5
MBC values (μg/mL) of silver NPs in different synthesis time against SA							
1:4	20	20	10	10	5	5	5
1:8	20	20	10	10	5	5	5

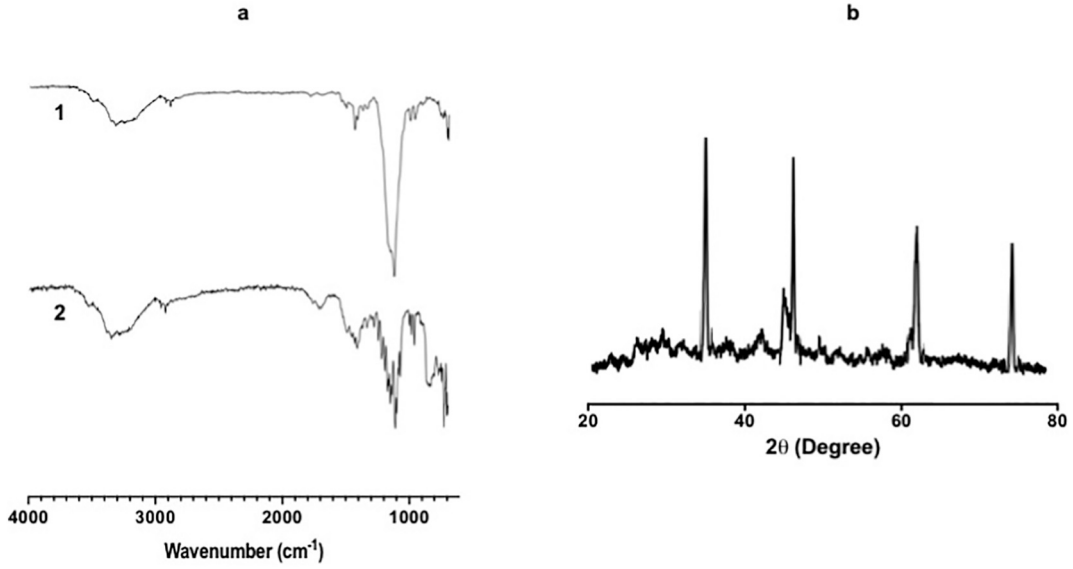

Fig. 4. FTIR spectra of green tea extract (1) and silver NPs (2) (**a**). X-ray diffractogram of silver NPs (**b**). (For interpretation of the references to color in this figure legend, the reader is referred to the web version of this article.)

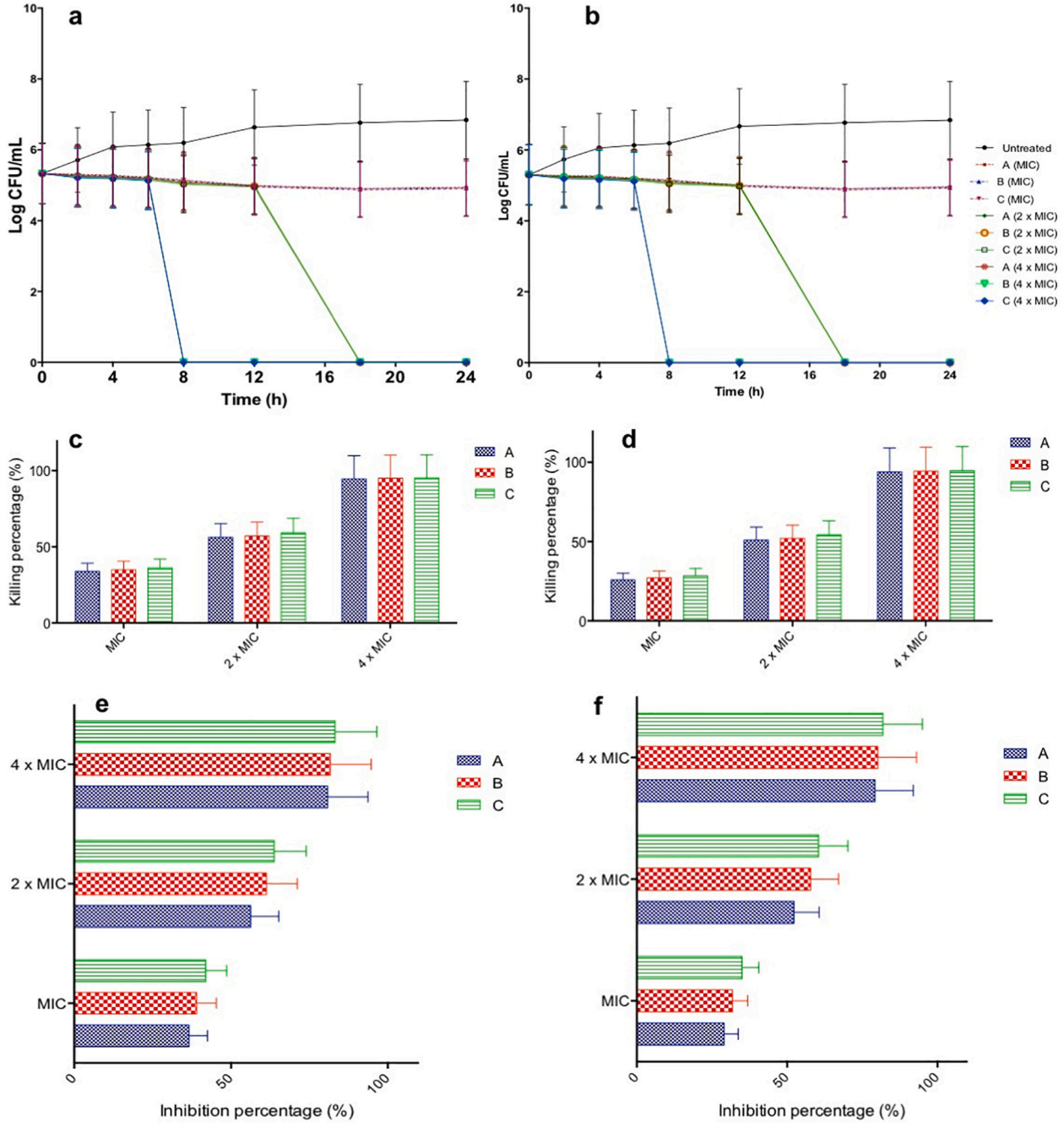

Fig. 5. Time kill assay of silver NPs against SA (**b**) and PA (**b**) (means ± SD, $n = 3$). Antibiofilm activity of silver NPs in 96-well microtiter against biofilms produced by SA (**c**) and PA (**d**) (means ± SD, $n = 3$). Antibiofilm activity of silver NPs in CBM models produced by SA (**e**) and PA (**f**) (means ± SD, $n = 3$).

presence of crystalline Ag [48]. Accordingly, it showed that the NPs obtained were comprised of crystalline Ag.

3.2. In vitro antibacterial activities

3.2.1. Determination of minimum inhibitory concentration and minimum bactericidal concentration

The antibacterial activities of silver NPs were further evaluated. The MIC and MBC values of silver NPs prepared using different synthesis times are shown in Table 3. The lowest MIC, indicating strong antibacterial activity, was shown by silver NPs prepared from the ratios 1:4 and 1:8. Moreover, MIC values were lower than corresponding MBC values. Accordingly, in order to kill the bacteria, the higher concentration of silver NPs was required. The ratio of MBC to MIC was less than 4, indicating that the silver NPs formed in this study possessed bactericidal ability. It has been reported that a ratio of >4 indicates bacteriostatic activity and a ratio of ≤4 indicates bactericidal activity [56]. The mechanism of action of silver NPs as antibacterial agents has been proposed to be mainly due to their ability to disturb membrane permeability. The disruption of cell membrane leads to leakage of intracellular content, resulting in damage of DNA and death of bacterial cells [57]. In this study, to minimize the use of green tea extract, as the MIC and MBC values of silver NPs prepared from the ratios 1:4 and 1:8 were found to be similar, the ratio of $AgNO_3$ and extract of 1: 4 was selected for further studies. Moreover, considering the MIC values, the synthesis times of 4 h, 5 h and 6 h were also used in the further studies.

3.2.2. Time kill assay

Following MIC and MBC determination, it was also crucial to investigate the time required by silver NPs to completely kill the bacterial cultures. Therefore, a time kill assay was conducted. Fig. 5a and b show the curves presenting the time required by silver NPs to kill SA and PA. The viable bacterial counts increased by approximately 7.1 log CFU in the untreated cohort following 1-day incubation time. In all cases, silver NPs with MIC values could not kill 99.99% of bacterial culture following 24 h incubation time. On the other hand, around 100% bacterial cultures were killed following the incubation with silver NPs at the concentration of twice of the MIC values after 18 h. Furthermore, within only 8 h, all bacteria were killed after incubation with 4 times the MIC values of silver NPs in all cases. Therefore, this evaluation indicated that the ability of silver NPs in killing the bacterial cultures was concentration dependent.

3.3. In vitro antibiofilm activities

3.3.1. 96-Well microtiter plate (MTP) biofilm study

Bacterial biofilms are able to reduce susceptibility of bacteria to antibacterial compounds [58]. To further evaluate the capability of silver NPs to eradicate the biofilms, *in vitro* antibiofilm was performed in 96-Well microtiter plate. Fig. 5c and d exhibit the percentages of reduction of bacterial biofilm after the application of silver NPs. With MIC values, silver NPs synthesized for 4 h, 5 h and 6 h were only able to eradicate 46.28 ± 5.13%, 47.98 ± 6.19% and 49.62 ± 4.98% of biofilms formed by SA and 32.91 ± 4.19%, 34.71 ± 4.87% and 35.87 ± 5.19% of biofilms formed by PA, respectively. Furthermore, 56.87 ± 6.28%, 58.77 ± 5.98% and 60.61 ± 8.39% of biofilms formed by SA, and 48.76 ± 5.87%, 50.98 ± 6.53% and 51.87 ± 7.87% of biofilms formed by PA were killed following incubation in the concentration of two times of MIC of silver NPs. Interestingly, in the case of silver NPs with the concentrations of four times of MIC, more than 95% of bacterial biofilms were killed after incubation with these NPs. Analyzed statistically, there were no significant different ($p > 0.05$) in antibiofilm activity of silver NPs synthesized for 4 h, 5 h and 6 h. Therefore, silver NPs synthesized in this study possessed antibiofilm activity *in vitro*.

3.3.2. Colony biofilm model (CBM)

In addition to antibiofilm evaluation in MTP, antibiofilm activities of silver NPs were also evaluated in a colony biofilm model (CBM). CBM model represents biofilm of bacteria prepared from a poly(carbonate) membrane as a substrate for the development of bacterial biofilms. The biofilm developing in this membrane resembles biofilm growth in a wound [2,59]. In addition, the environment of wounds could be easily imitated due to the small fluid shear and the nearness to an air boundary created by this system [60]. The agar media used contained carbon and nitrogen which are similar to the nutrients present in biofilms of a wound [2]. The viable bacteria can be easily counted in this model. After antibiofilm studies, the membrane can be detached from the agar and bacteria can be resuspended in the broth medium for viable bacterial count determination. The results of this evaluation are depicted in Fig. 5e and f. In this study, in MIC values, silver NPs synthesized for 4 h, 5 h and 6 h were only able to kill 41.21 ± 4.19%, 43.91 ± 5.21% and 46.76 ± 4.87% of CBMs formed by SA and 30.12 ± 3.92%, 31.43 ± 3.94% and 34.32 ± 4.54% of CBMs formed by PA, respectively. Furthermore, following incubation in the concentration of two times of MIC of silver NPs, more than 50% of biofilms formed by SA and PA in CBM were killed. Interestingly, more than 85% of bacterial biofilms in CBM were eradicated after incubation with the concentrations of four times of MIC of silver NPs. These results showed the effectiveness silver NPs in killing the mature bacterial biofilms. When analyzed statistically, there was no significant difference ($p > 0.05$) in antibiofilm activity in CBM of silver NPs synthesized for 4 h, 5 h and 6 h. Accordingly, for the efficiency, 4 h was selected as the optimum synthesis time of silver NPs.

Table 4
Particle size, SPAN value, zeta potential, encapsulation efficiency and drug loading capacity of different formulations of silver NPs loaded MPs (means ± SD, $n = 3$).

Formulations	Particle size (μm)	SPAN	Zeta potential	EE (%)	LC (%)
MP1	1.76 ± 0.11	0.81 ± 0.05	17.32 ± 1.87	18.21 ± 1.98	8.65 ± 0.92
MP2	2.18 ± 0.26	0.83 ± 0.07	23.61 ± 2.32	32.76 ± 3.19	11.76 ± 1.19
MP3	2.65 ± 0.31	0.86 ± 0.07	31.21 ± 2.71	38.32 ± 4.32	16.19 ± 1.59
MP4	2.81 ± 0.27	0.89 ± 0.09	35.73 ± 3.11	52.76 ± 4.98	16.46 ± 1.71
MP5	5.32 ± 0.61	0.95 ± 0.12	36.19 ± 4.01	59.17 ± 5.14	15.03 ± 1.48

3.4. Formulation and characterization of PCL MPs loaded with silver NPs

Silver NPs loaded MPs were prepared using a solvent/non-solvent technique with PVP as stabilizer. In this study, PCL was used as MP matrix, coated with chitosan. In our previous study, we have shown that, compared to non-coated PCL nanoparticles, PCL nanoparticles coated with chitosan resulted in higher antibiofilm activity [26]. The surface of biofilm EPS and cell walls of bacteria have been found to be negatively charged. Therefore, the decoration using chitosan, having positive surface charge, could increase the attraction to infected sites [28]. The characteristics of MPs are depicted in Table 4. The results show that the increase on PCL amounts increased the particle size of MPs. The particle sizes obtained were found to be 1.76 ± 0.11 μm for MP1, 2.18 ± 0.26 μm for MP2, 2.65 ± 0.31 μm for MP3, 2.81 ± 0.27 μm for MP4 and 5.32 ± 0.61 μm for MP5. There was significant difference ($p < 0.05$) in particle size of MP1 compared to all other formulations. Specifically, there was no significant different ($p > 0.05$) in particle size between MP3 and MP4. The SPAN values were in the range of 0.81 ± 0.05 and 0.95 ± 0.12, indicating narrow distribution of MPs obtained. Analyzed statistically, there was no significant difference ($p > 0.05$) in SPAN values of all formulations. For zeta potential, the values were 17.32 ± 1.87 mV for MP1, 23.61 ± 2.32 mV for MP2, 31.21 ± 2.71 mV for MP3, 35.73 ± 3.11 mV for MP4 and 36.19 ± 4.01 mV for MP5. In all cases, the zeta potentials were found to be positive. The positive zeta potentials may be caused by the presence of positive amine groups in the chitosan [61], Interestingly, MP3, MP4 and MP5 showed zeta potential values of >30 mV. These values could potentially maintain the physical stability and avoid the agglomeration of MPs during the storage [54].

With respect to the EE of silver NPs into PCL MPs, it was found that the EE values were between 18.21 ± 1.98% and 69.17 ± 7.14%. The EE of MP1 (18.21 ± 1.98%) was significantly lower ($p < 0.05$) compared to other formulations. The increase of PCL concentration in the formulations also increased the EE values. The EE value of MP4 (52.76 ± 4.98%) was found to be significant higher ($p < 0.05$) than MP3 (38.32 ± 4.32%) and MP2 (32.76 ± 3.19%). However, the increase of PCL amount in MP5 did not significantly increase ($p > 0.05$) the EE value (59.17 ± 5.14%) of silver NPs into MPs. Regarding the LC, the values were between 8.65 ± 0.92% and 16.46 ± 1.71%. MP4 showed the highest LC value (16.46 ± 1.71%) in comparison with other formulations.

SEM images showing the morphologies of silver NPs loaded MPs are presented in Fig. 6a–e. The results showed that the sizes of all formulations were in close agreement with the results obtained from particle sizes measurement. Particles were approximately spherical in shape.

3.5. In-vitro release study of silver NPs from MPs in bacterial cultures

The primary aim of this study was to specifically develop bacterially responsive MPs to selectively deliver silver NPs to infected sites. Accordingly, the release profiles of silver NPs from MPs were evaluated with and without the presence the SA and PA cultures as biofilm former

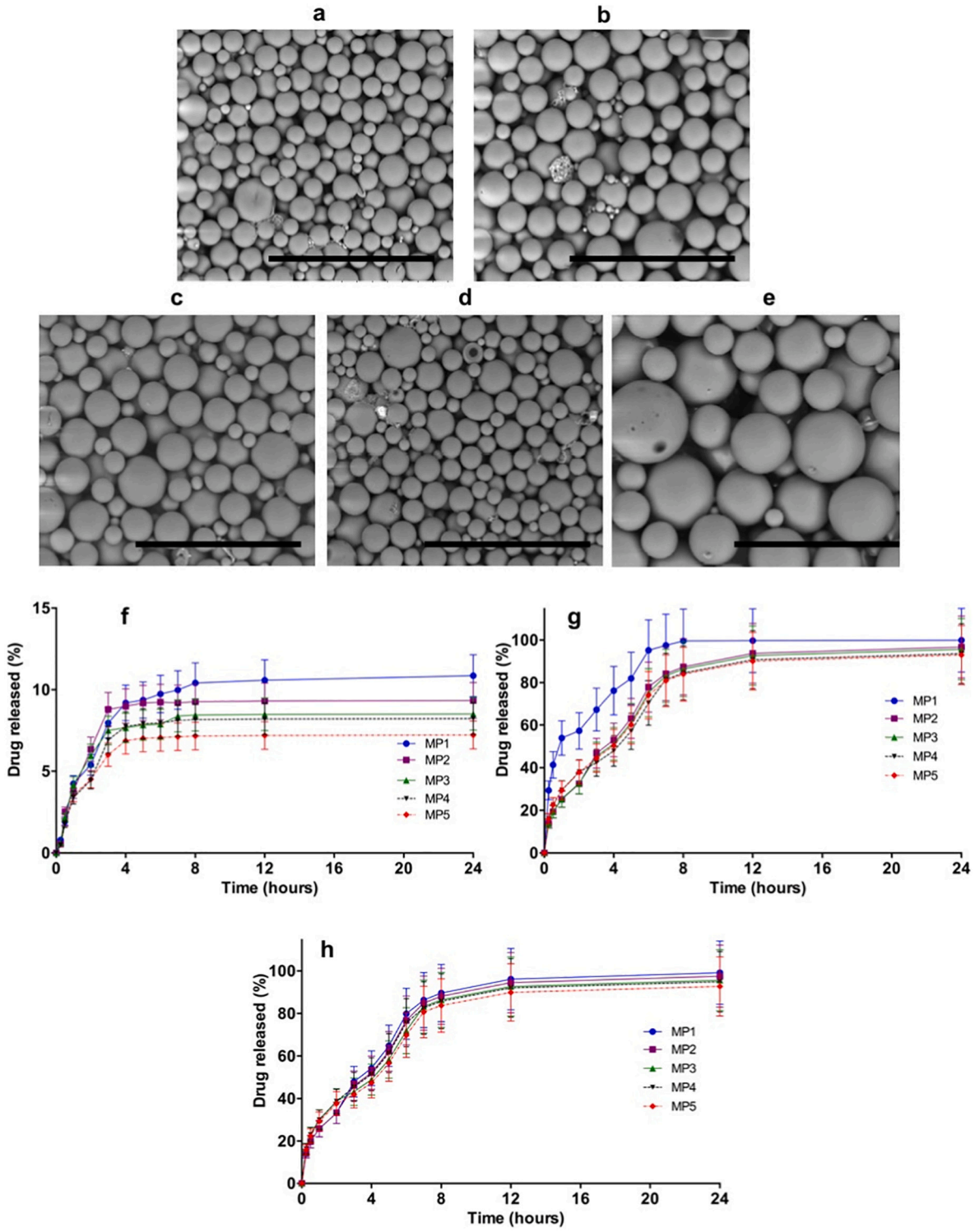

Fig. 6. SEM images of MP1 (**a**), MP2 (**b**), MP3 (**c**), MP4 (**d**) and MP5 (**e**) at a magnification power of 30,000×. (The black scale bar represents a length of 10 μm in each case). *In-vitro* release of silver NPs from MPs in the absence of bacterial culture (**f**) and presence of SA (**g**) and PA (**h**) (mean ± S.D., $n = 3$).

bacterial. Without bacterial cultures, all MP formulations were only able to release less than 15% of silver. After 24 h, only 10.27 ± 1.21%, 9.65 ± 1.11%, 8.54 ± 1.13%, 8.32 ± 1.18% and 7.19 ± 0.87% of silver were released from MP1, MP2, MP3, MP4 and MP5, respectively (Fig. 6f). On the other hand, around 100% of silver were released from all MPs in the presence of SA and PA. Specifically, following 24 h, the releases of silver were found to be 99.88 ± 14.32% from MP1, 96.76 ± 13.21% from MP2, 95.68 ± 14.33 from MP3, 93.65 ± 12.98% from MP4 and 92.95 ± 13.94% from MP5 in the presence of SA (Fig. 6g). With respect to the releases of silver in PA cultures, the total release percentages were 99.18 ± 13.54%, 97.53 ± 14.65%, 95.62 ± 12.11%, 94.91 ± 14.21% and 92.63 ± 12.87% from MP1, MP2, MP3, MP4 and MP5, respectively (Fig. 6h). Analyzed statistically, there was no significant difference ($p > 0.05$) in the release of silver from all MP formulations in both bacterial cultures.

The findings attained in these studies revealed that the incorporation

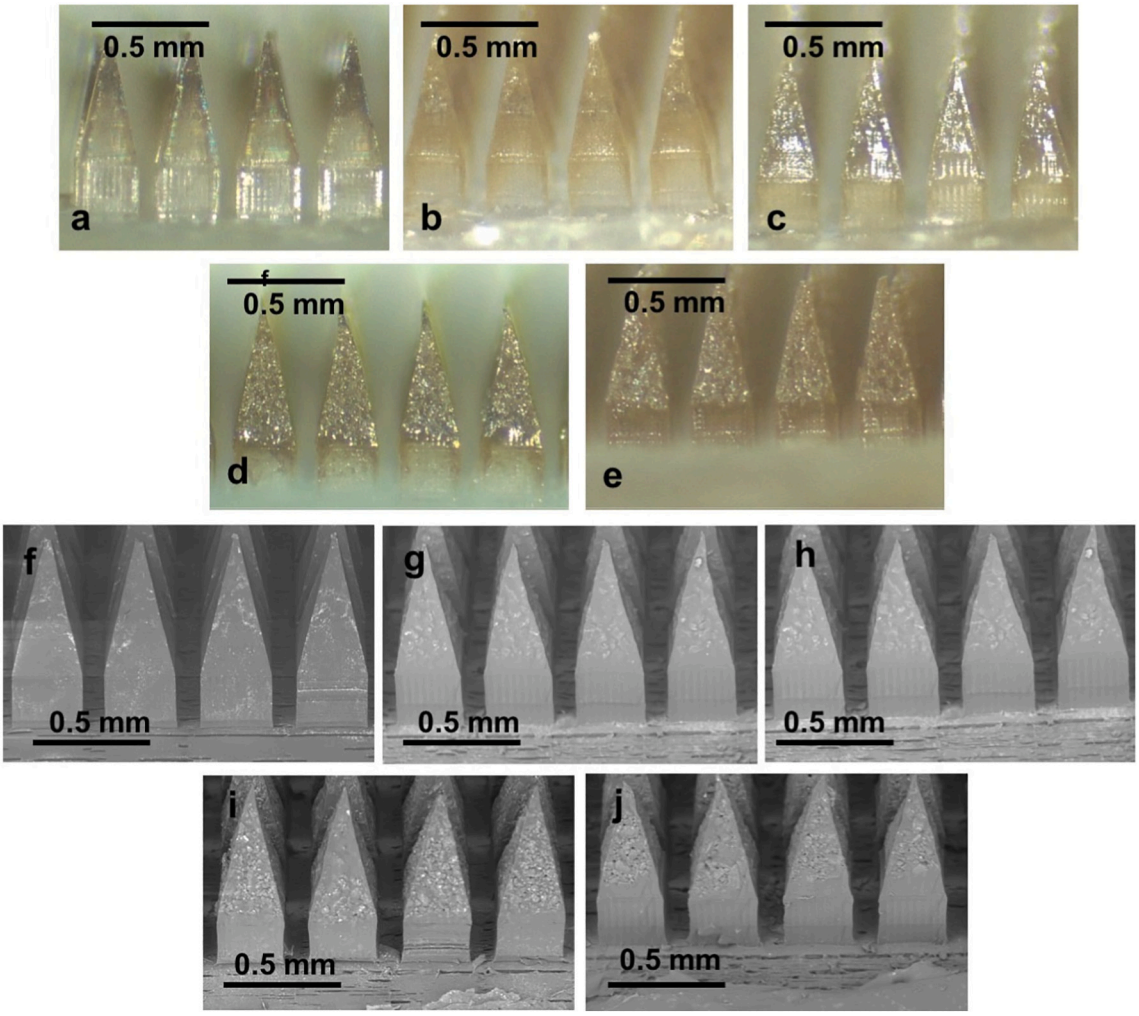

Fig. 7. Light microscope images of the DMN formulations containing 10% w/w of dry MPs: 90% w/w of MN matrix (F1) (**a**), 20% w/w of dry MPs: 80% w/w of MN matrix (F2) (**b**), 30% w/w of dry MPs: 70% w/w of MN matrix (F3) (**c**), 40% w/w of dry MPs: 60% w/w of MN matrix (F4) (**d**) and 50% w/w of dry MPs: 60% w/w of MN matrix (F5) (**e**). Free DOX (**1**), NP-1 (**2**), NP-2 (**3**), NP-3 (**4**) and NP-4 (**5**) and NP-5 (**6**). SEM images of the DMN formulations containing 10% w/w of dry MPs: 90% w/w of MN matrix (F1) (**f**), 20% w/w of dry MPs: 80% w/w of MN matrix (F2) (**g**), 30% w/w of dry MPs: 70% w/w of MN matrix (F3) (**h**), 40% w/w of dry MPs: 60% w/w of MN matrix (F4) (**i**) and 50% w/w of dry MPs: 60% w/w of MN matrix (F5) (**j**).

of silver NPs into PCL MPs led to the selective release of silver NPs in the presence of biofilm-forming bacterial cultures. Accordingly, this delivery system could possibly be favorable for enabling delivery only at the infection site, circumventing the non-specific exposure to uninfected areas. The selective release from MPs might be due to the use of polymers in this study. PCL used in this study has been reported to be degraded by lipase enzymes produced by SA and PA. Xiang et al. (2012) found the rapid release of vancomycin from PCL nanogels in the presence of this bacteria. Importantly, the release of vancomycin was significantly lower without the bacterial culture [27]. Our previous study has also shown that the releases of DOX from non-decorated PCL formulations and PCL formulations coated with chitosan in the presence of bacterial cultures were significantly higher compared to those without bacterial cultures [26]. The same approach was also used to develop responsive NPs of carvacrol [62]. Moreover, the coating agent used, chitosan, has been also found to be degraded by the lipase enzyme [63]. Therefore, we successfully developed silver NPs loaded PCL MPs coated with chitosan for bacteria sensitive release. Considering our result in the characterization step, MP4 was selected for further studies.

3.6. Fabrication of two-layered DMNs

In skin infection associated with biofilm formation, the delivery of antibacterial compounds has been hindered by the formation of an extracellular polymeric substance. Therefore, to improve the penetration of the antibacterial agents and disturb the biofilm matrix, the silver NPs loaded MPs were further formulated into DMN arrays. The mixture of two water soluble polymers, namely PVA and PVP were used to prepare the DMNs. In our previous studies, the use of single polymer was not able to produce DMNs with sufficient mechanical properties [34,36]. On the other hand, when combined, C=O groups of PVP and -OH groups of PVA form the hydrogen bond, increasing the mechanical strength of DMNs [36]. In this study, to attain the maximum possible drug loading, a plethora of numerous DMN formulations were prepared with different MPs concentrations. The morphologies of all DMN formulations observed by light microscope and SEM are shown in Fig. 7, revealing that all DMNs obtained formed sharp needles. Hence, all formulations were characterized in further experiments.

3.7. Evaluation of mechanical and insertion properties of DMNs

The incorporation of other compounds has been found to affect, either in strengthening or weaking, the DMN formulations [64]. The initial characterization for DMNs was the mechanical strength evaluation. This study was performed to evaluate the ability of DMNs in resisting compression. The mechanical property was assessed by

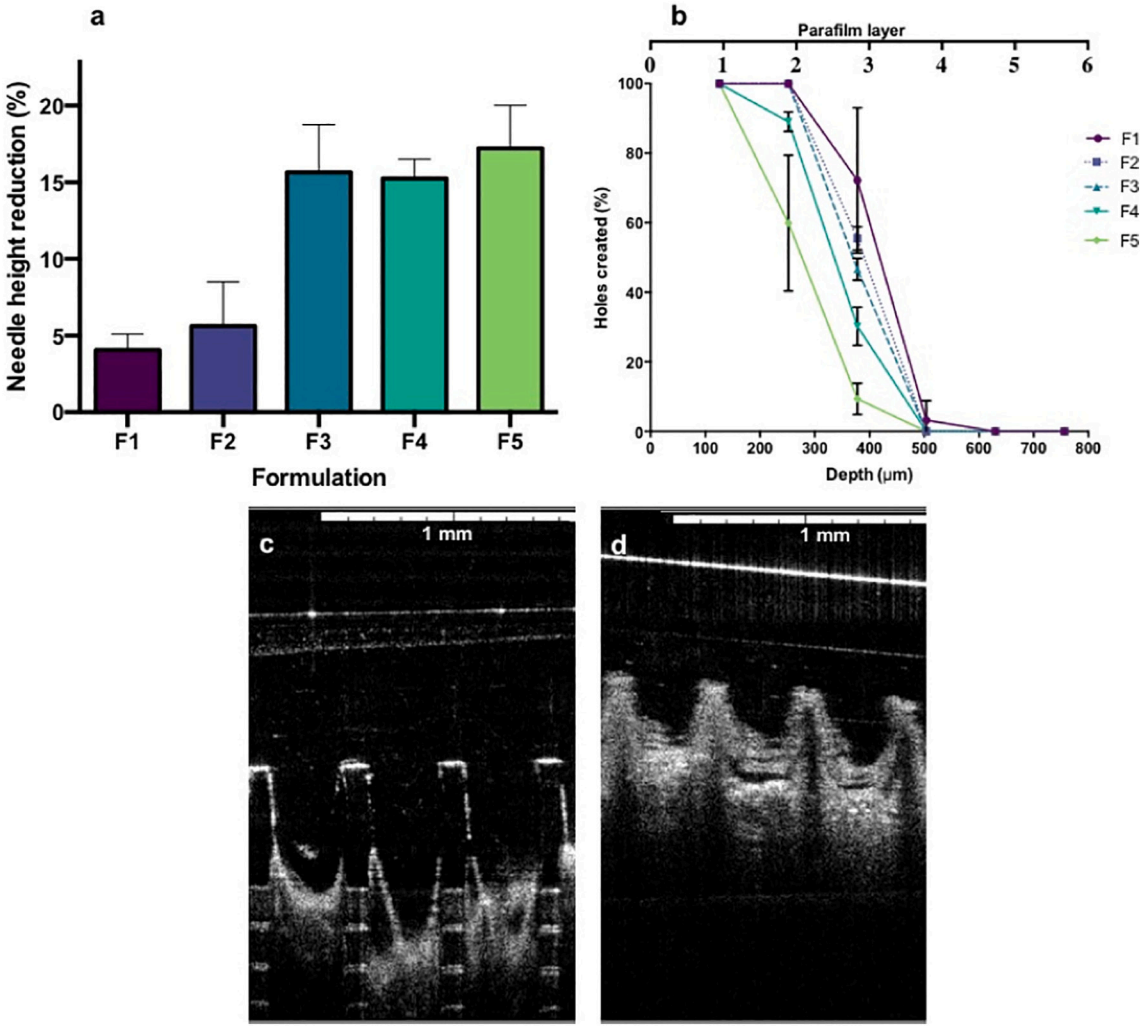

Fig. 8. The percentage height reduction of needles on the various DMN arrays (means ± SD, $n = 3$) (**a**). Percentage of holes created in Parafilm®M layers, using an insertion force of 32 N/array for the various DMN arrays (means ± SD, $n = 3$) (**b**). Representative OCT images of F3 after insertion into Parafilm®M film (**c**) and full-thickness porcine skin (**d**). The scale bar represents a length of 1 mm in each case.

calculating the height reduction following the compression with a force of 32 N/DMN array. This pressure was reported to be equal to human manual pressure [44]. The percentage of height reduction of all formulations, representing the mechanical properties is depicted in Fig. 8a. The reductions in MN height were 4.06 ± 1.03% for F1, 5.60 ± 2.89% for F2, 15.64 ± 3.11% for F3, 15.25 ± 1.26% for F4 and 17.22 ± 2.80% for F5. There was no significant difference ($p > 0.05$) in height reduction between F1 and F2. These values were significantly higher ($p < 0.05$) compared to those values in F3, F4 and F5. Furthermore, there were no significant ($p > 0.05$) differences in height reduction between F3, F4 and F5. Although the percentage of height reduction of F3 and F4 were found to be higher than F2 and F3, some studies showed that a percentage of height reduction of around 25% was acceptable in DMN formulations [65].

The ability of a DMN array to be successfully inserted into the skin is crucial to its utility. Therefore, the insertion property evaluation was performed, using eight-layers of Parafilm®M. Fig. 8b presents the insertion properties of all DMN formulations in Parafilm®M, presented as the percentage of holes created in Parafilm®M. The trend of the insertion properties evaluation was similar to the mechanical properties, showing that the higher concentration of MPs loaded into DMNs decreased the insertion ability of DMNs. However, all formulations penetrated three layers of Parafilm®M. The mean thickness of each layer of Parafilm®M is 126 μm. Therefore, the DMNs were inserted up to 378 μm. In the third layer, 72.12 ± 25.88%, 55.47 ± 3.40%, 46.62 ± 3.16%, 30.21 ± 5.48% and 9.38 ± 4.51% of holes created by F1, F2, F3, F4 and F5, respectively. Analyzed statistically, the holes created by F4 and F5 were significantly lower ($p < 0.05$) than those by F1, F2 and F3. Furthermore, there were no significant differences ($p > 0.05$) in the holes created by F1, F2 and F3. Therefore, as F3 contained higher concentration of MPs, this formulation was selected for further evaluations. To support these results, the insertion profile of F3 in the Parafilm®M and the full-thickness neonatal porcine skin models was then evaluated using optical coherence tomography (OCT). Several studies have shown the effectiveness of this technique to observe the insertion ability of various MN formulations [43,66–70]. The OCT images of insertion of F3 into the Parafilm®M and the full-thickness neonatal porcine skin are depicted in Fig. 8c and d, respectively, showing that this formulation was successfully inserted in both models.

3.8. *Ex vivo* dermatokinetic studies

A dermatokinetic study was then carried out to investigate the release kinetic of silver NPs from MPs following DMN applications. This study was performed in non-infected skin and *ex vivo* model of biofilms in rat skins. To confirm that the release of silvers in the skin was only influenced by the presence of bacterial biofilms former, only silvers released from MPs were quantified. To achieve this, the skin samples

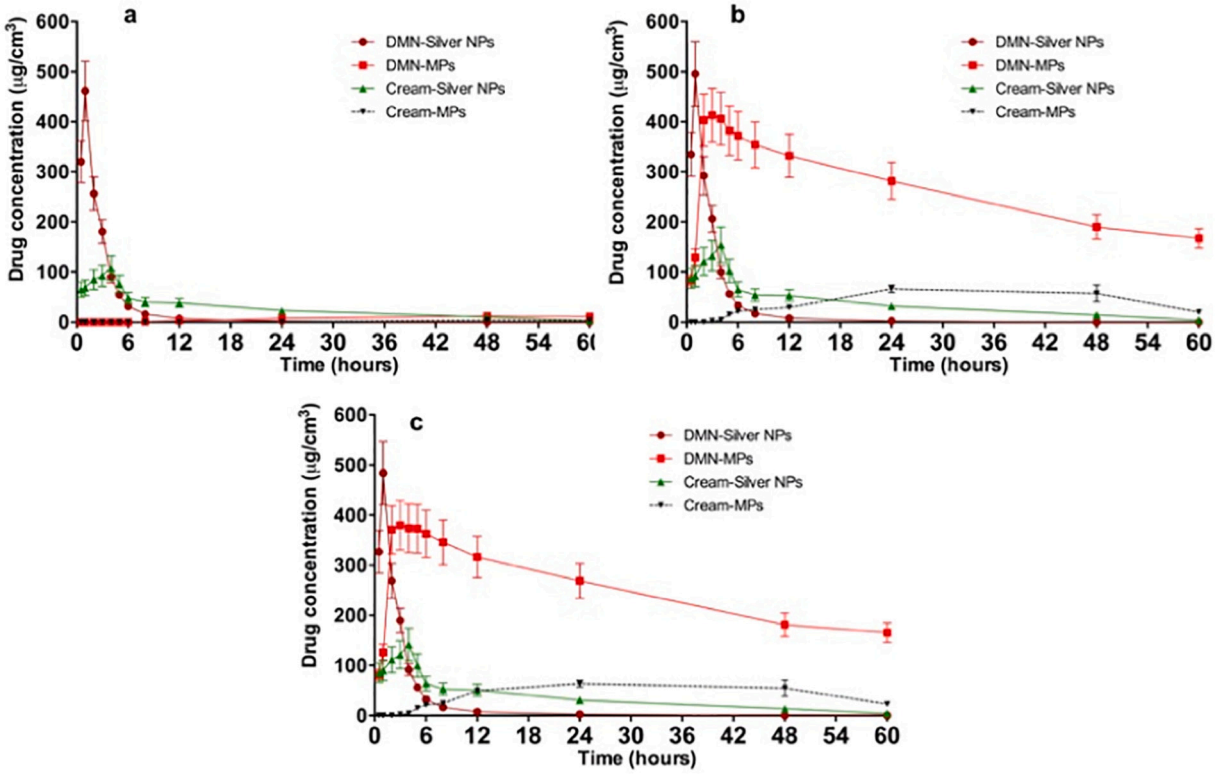

Fig. 9. The *ex vivo* concentrations and time profiles of silver NPs in non-infected rat skin (**a**), as well as *ex vivo* biofilm models formed by SA (**b**) and PA (**c**) following the application of DMN-Silver NPs, DMN-MPs, cream-Silver NPs and cream-MPs. (means ± S.D., $n = 3$).

Table 5
Dermatokinetic parameters of silver NPs in non-infected rat skin, as well as *ex vivo* biofilm models formed by SA and PA following the application of DMN-Silver NPs, DMN-MPs, cream-Silver NPs and cream-MPs. (means ± S.D., $n = 3$).

Condition	Formulation	C_{max} (µg/cm^3)	T_{max} (h)	$T_{1/2}$ (h)	AUC (h·µg/cm^3)	MRT (h)
Normal skin	DMN-Silver NPs	503 ± 64.32	0.89 ± 0.12	1.38 ± 0.01	1687.83 ± 343.56	2.99 ± 0.39
	DMN-MPs	8.42 ± 1.43	72.18 ± 10.32	60.54 ± 6.89	499.65 ± 99.82	159.72 ± 29.53
	Cream-Silver NPs	110.31 ± 21.32	8.32 ± 1.98	24.69 ± 2.83	879.32 ± 106.26	138.16 ± 20.12
	Cream-MPs	4.32 ± 0.87	69.20 ± 9.32	58.47 ± 7.53	277.54 ± 59.98	129.85 ± 17.98
Biofilm model by SA	DMN-Silver NPs	499.87 ± 53.41	0.76 ± 0.09	1.32 ± 0.02	1765.62 ± 299.88	3.11 ± 0.42
	DMN-MPs	423.98 ± 58.65	3.87 ± 0.21	36.19 ± 5.31	23,468.71 ± 3198.75	65.65 ± 7.33
	Cream-Silver NPs	164.31 ± 31.23	4.98 ± 0.71	29.54 ± 4.85	647.25 ± 99.08	31.30 ± 4.42
	Cream-MPs	69.32 ± 7.98	28.32 ± 5.12	31.98 ± 5.24	196.37 ± 23.21	44.21 ± 5.21
Biofilm model by PA	DMN-Silver NPs	491.76 ± 62.31	0.82 ± 0.18	1.43 ± 0.02	1698.37 ± 388.76	2.34 ± 0.33
	DMN-MPs	403.13 ± 49.29	3.76 ± 0.28	38.65 ± 5.54	21,988.29 ± 3069.32	64.61 ± 6.32
	Cream-Silver NPs	159.17 ± 28.45	4.71 ± 0.69	27.87 ± 3.65	607.88 ± 110.43	30.21 ± 4.99
	Cream-MPs	64.32 ± 4.32	27.13 ± 3.43	33.86 ± 5.67	189.47 ± 28.76	42.21 ± 6.15

were vortexed with water at each time interval. Moreover, this technique was employed to silver NPs loaded MP dispersions to assess whether this technique could disturb the MPs. Our findings displayed that there was no silver found in the supernatant of MP dispersions. Therefore, this technique could only extract silvers released from MPs.

In this study, the dermatokinetic profile of our approach was compared to DMNs containing silver NPs without MP formulation (DMN-silver NPs). Additionally, the dermatokinetic profiles of a conventional cream containing silver NPs (cream-silver NPs) and silver NPs loaded MPs (cream-MPs) were also evaluated. The kinetic profiles of silver NPs in the normal skin and the *ex vivo* biofilm models, illustrated as the concentration of silvers released from MPs in the skin *versus* the application time, after the application of the DMNs and conventional cream of silver NPs and silver NPs loaded MPs are presented in Fig. 9. The dermatokinetic profiles, including C_{max}, T_{max}, $T_{1/2}$, AUC and MRT, of silvers after the application of the DMNs and conventional cream of silver NPs and silver NPs loaded MPs are presented in Table 5. As depicted, without the presence of bacterial culture in the normal skin, the release of silvers from DMNs-MPs and cream-MPs was significantly lower ($p < 0.05$) compared to DMN-silver NPs and cream-silver NPs. This indicated that the non-specific release of silver NPs could be potentially circumvented by the incorporation of silver NPs into MPs. On the other hand, in *ex vivo* biofilm models generated from SA and PA, the release of silver NPs from DMN-MPs was significantly enhanced ($p < 0.05$) in comparison with DMN-silver NPs, cream-silver NPs and cream-MPs.

With respect to AUC, the AUC values of silver NPs from DMN-MPs in the both *ex vivo* biofilm models were found to be significantly higher ($p < 0.05$) compared to other formulations, indicating an excellent *ex vivo* skin bioavailability of our approach. In the case of the retention time in the skin, it was found that the MRT values of silver Ns from DMN-MPs were significantly greater ($p < 0.05$) than those of DMN-silver NPs, DMN-MPs, cream-silver NPs and cream-MPs. The higher MRT could be favorable to decrease the application time of silver NPs in treatment of

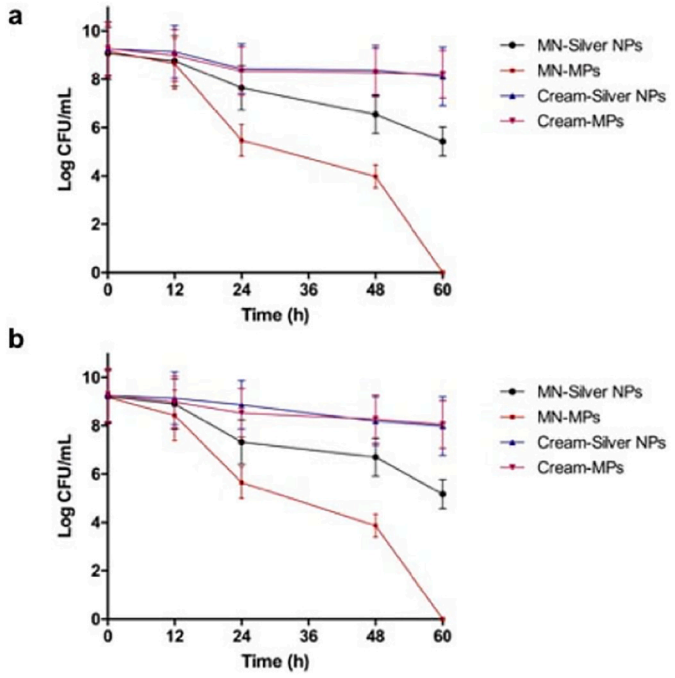

Fig. 10. Bacterial viability (log CFU/mL) on in *ex vivo* biofilm models formed by SA (a) and PA (b) following the application of DMN-Silver NPs, DMN-MPs, cream-Silver NPs and cream-MPs. (means ± S.D., $n = 3$).

skin infection associated with biofilm formation. Hence, it could result in patient acceptability of this approach. From our results, it was concluded that the combination approach of responsive MPs and DMNs could lead to the successful delivery of silver NPs into *ex vivo* biofilm model.

3.9. Antibiofilm activity in ex vivo model of biofilm on rat skin

In an attempt to assess the efficacy of this approach, the decrease of bacterial bioburdens in an *ex vivo* biofilm models produced from SA and PA were investigated by counting the viable cell counts. The results of this study are shown in Fig. 10. In both *ex vivo* biofilm models, the lowest antibiofilm activity was achieved after the application of cream-silver NPs, with only around 50% of bacterial bioburden reduction after 48 h. The incorporation of silver NPs into MPs, which were formulated into cream conventional, was able to improve the *ex vivo* antibiofilm activity by around 10% to approximately 60% of bacterial bioburden reduction after 24 h application. This result was in a good agreement with the dermatokinetic studies, showing that cream-MPs exhibited better dermatokinetics than cream-silver NPs. Furthermore, following the incorporation into DMNs, the application of silver NPs to the *ex vivo* biofilm models in both bacterial resulted in more than 75% reduction of bacterial bioburden after 60 h treatment. This implied that DMNs could potentially increase the efficacy of silver NPs as antibiofilm agents. Several studies have shown that the incorporation of antibacterial agents into MNs led to an increase in antibacterial activity [26,40,71]. Essentially, because DMN-MPs exhibited the highest *ex vivo* skin bioavailability in the dermatokinetic studies, the application of this approach was able to eradicate 100% of the biofilms of SA and PA. Hence, the administration of silver NPs loaded with PCL-chitosan MPs delivered by DMNs led to two main benefits. Firstly, this approach was able to enhance and control the dermatokinetic profiles of silver NPs. Also, this approach could improve the efficacy of silver NPs in *ex vivo* biofilm model in rat skin formed by SA and PA, in comparison with DMNs without MP formulations, as well as conventional cream formulation containing silver NPs and silver NPs loaded with MPs.

The promising results of this study have proven the concept of the study that the responsive MPs laden with silver NPs can be effectively delivered into the skin using DMNs and, afterwards, NPs can display their antimicrobial activity at the area of infection. The overriding benefits of the selective delivery system we have developed here, in comparison with conventional cream dosage form, lies in the capability for site-selective delivery and long retention time in the area of infection in the skin which could potentially enhance the efficacy of antibacterial therapy of burns and chronic wounds. DMNs could, hence, be used for the delivery of antimicrobial agents topically to wounds, and their combination with selective MPs could be a feasible alternative to the current antimicrobial managements.

4. Conclusion

This extensive study has shown the feasibility to encapsulate silver NPs into responsive MPs prepared from PCL and chitosan. Delivered by DMN approach, this combination could be an alternative choice to overcome the problem in the therapy of skin infection associated with bacterial biofilms. Leading on from this, several further studies are highly recommended. As one of the reasons of the development of this approach was due to the toxicity issue of silver NPs, toxicity studies must be performed. Importantly, the ability to eradicate biofilm should be performed in *in vivo* study using an appropriate animal model. Additionally, before this combination delivery system can achieve clinical application and reach patient benefit, the studies regarding usability and acceptability of this device should be performed to confirm maximum effect of the work.

Author contribution statement

Andi Dian Permana: Conceptualization, Methodology, Writing - Original Draft, Investigation, Data Curation, Project Administration, Funding Acquisition, Supervision; **Qonita Kurnia Anjani**: Methodology, Investigation, Data Curation; **Sartini**: Conceptualization, Project Administration, **Emilia Utomo**: Methodology, Investigation, Data Curation; **Fabiana Volpe-Zanutto**: Methodology, Review & Editing; **Alejandro J. Paredes**: Methodology, Review & Editing; **Yayu Mulsiani Evary**: Methodology, Review & Editing; **Sandra Aulia Mardikasari**: Methodology, Review & Editing; **Muh. Rezky Pratama**: Methodology, Investigation; **Irma Nurfadilah Tuany**: Methodology, Investigation; **Ryan F. Donnelly**: Conceptualization, Methodology, Review & Editing, Project Administration, Funding Acquisition.

Declaration of competing interest

The authors declare that they have no known competing financial interests or personal relationships that could have appeared to influence the work reported in this paper.

Acknowledgments

The authors wish to thank Hasanuddin University (Penelitian Dasar Universitas Hasanuddin 1585/UN.4.22/PT.01.03/2020) for supporting this work. This study was also supported in part by Wellcome Trust grant number WT094085MA. Additionally, authors thank Luki Ahmadi Hari Wardoyo for his support designing the figures in this manuscript.

References

[1] K. Moore, R. McCallion, R.J. Searle, M.C. Stacey, K.G. Harding, Prediction and monitoring the therapeutic response of chronic dermal wounds, Int. Wound J. 3 (2006) 89–96.

[2] I.S. Blagbrough, N. Alhusein, M.L. Beeton, A. Bolhuis, P.A. De Bank, Electrospun Zein/PCL fibrous matrices release tetracycline in a controlled manner, killing Staphylococcus aureus both in biofilms and ex vivo on pig skin, and are compatible with human skin cells, Pharm. Res. 33 (2016) 237–246.

[3] A.A. Hammond, K.G. Miller, C.J. Kruczek, J. Dertien, J.A. Colmer-Hamood, J. A. Griswold, A.R. Horswill, A.N. Hamood, An in vitro biofilm model to examine the effect of antibiotic ointments on biofilms produced by burn wound bacterial isolates, Burns. 37 (2011) 312–321.

[4] H. El-Mohri, Y. Wu, S. Mohanty, G. Ghosh, Impact of matrix stiffness on fibroblast function, Mater. Sci. Eng. C. 74 (2017) 146–151.

[5] M.M. Mihai, M. Preda, I. Lungu, M.C. Gestal, M.I. Popa, A.M. Holban, Nanocoatings for chronic wound repair—modulation of microbial colonization and biofilm formation, Int. J. Mol. Sci. 19 (2018).

[6] N.B. Haidar, S. Marais, E. Dé, A. Schaumann, M. Barreau, M.G.J. Feuilloley, A.C. Duncan, Chronic wound healing: A specific antibiofilm protein-asymmetric release system, Mater. Sci. Eng. C. 106 (2020).

[7] P.F. Duckworth, R.S. Rowlands, M.E. Barbour, S.E. Maddocks, A novel flow-system to establish experimental biofilms for modelling chronic wound infection and testing the efficacy of wound dressings, Microbiol. Res. 215 (2018) 141–147.

[8] M. Clinmicrorevs, P. Bowler, D.G. Armstrong, Wound microbiology and associated approaches to wound, Clin. Microbiol. Rev. 14 (2001) 244–269.

[9] G.V. Doern, R.N. Jones, M.A. Pfaller, K.C. Kugler, M.L. Beach, Bacterial pathogens isolated from patients with skin and soft tissue infections: frequency of occurrence and antimicrobial susceptibility patterns from the SENTRY Antimicrobial Surveillance Program (United States and Canada, 1997), Diagn. Microbiol. Infect. Dis. 34 (1999) 65–72.

[10] H.C. Flemming, J. Wingender, The biofilm matrix, Nat. Rev. Microbiol. 8 (2010) 623–633.

[11] I. Olsen, Biofilm-specific antibiotic tolerance and resistance, Eur. J. Clin. Microbiol. Infect. Dis. 34 (2015) 877–886.

[12] K. Marion-Ferey, M. Pasmore, P. Stoodley, S. Wilson, G.P. Husson, J.W. Costerton, Biofilm removal from silicone tubing: an assessment of the efficacy of dialysis machine decontamination procedures using an in vitro model, J. Hosp. Infect. 53 (2003) 64–71.

[13] A.S. Lynch, G.T. Robertson, Bacterial and fungal biofilm infections, Annu. Rev. Med. 59 (2008) 415–428.

[14] R.D. Wolcott, K.P. Rumbaugh, G. James, G. Schultz, P. Phillips, Q. Yang, C. Waiters, P.S. Stewart, S.E. Dowd, Biofilm maturity studies indicate sharp debridement opens a timedependent therapeutic window, J. Wound Care 19 (2010) 320–328.

[15] S.B. Levy, M. Bonnie, Antibacterial resistance worldwide: causes, challenges and responses, Nat. Med. 10 (2004) S122–S129.

[16] K. Kalishwaralal, S. BarathManiKanth, S.R.K. Pandian, V. Deepak, S. Gurunathan, Silver nanoparticles impede the biofilm formation by Pseudomonas aeruginosa and Staphylococcus epidermidis, Colloids Surfaces B Biointerfaces. 79 (2010) 340–344, https://doi.org/10.1016/j.colsurfb.2010.04.014.

[17] A.R. Shahverdi, A. Fakhimi, H.R. Shahverdi, S. Minaian, Synthesis and effect of silver nanoparticles on the antibacterial activity of different antibiotics against Staphylococcus aureus and Escherichia coli, Nanomedicine Nanotechnology, Biol. Med. 3 (2007) 168–171, https://doi.org/10.1016/j.nano.2007.02.001.

[18] P. on Rujitanaroj, N. Pimpha, P. Supaphol, Wound-dressing materials with antibacterial activity from electrospun gelatin fiber mats containing silver nanoparticles, Polymer (Guildf). 49 (2008) 4723–4732. doi:https://doi.org/10.1016/j.polymer.2008.08.021.

[19] F. Esmaile, H. Koohestani, H. Abdollah-Pour, Characterization and antibacterial activity of silver nanoparticles green synthesized using Ziziphora clinopodioides extract, Environ. Nanotechnology, Monit. Manag. 14 (2020) 100303. doi:https://doi.org/10.1016/j.enmm.2020.100303.

[20] S. Ahmed, M. Ahmad, B.L. Swami, S. Ikram, A review on plants extract mediated synthesis of silver nanoparticles for antimicrobial applications: a green expertise, J. Adv. Res. 7 (2016) 17–28, https://doi.org/10.1016/j.jare.2015.02.007.

[21] J.Y. Song, B.S. Kim, Rapid biological synthesis of silver nanoparticles using plant leaf extracts, Bioprocess Biosyst. Eng. 32 (2009) 79–84, https://doi.org/10.1007/s00449-008-0224-6.

[22] S.S.K. Kamal, P.K. Sahoo, J. Vimala, M. Premkumar, S. Ram, L. Durai, A novel green chemical route for synthesis of silver nanoparticles using Camellia sinensis, Acta Chim. Slov. 57 (2010) 808–812.

[23] W.R. Rolim, M.T. Pelegrino, B. de Araújo Lima, L.S. Ferraz, F.N. Costa, J. S. Bernardes, T. Rodigues, M. Brocchi, A.B. Seabra, Green tea extract mediated biogenic synthesis of silver nanoparticles: characterization, cytotoxicity evaluation and antibacterial activity, Appl. Surf. Sci. 463 (2019) 66–74, https://doi.org/10.1016/j.apsusc.2018.08.203.

[24] C. Beer, R. Foldbjerg, Y. Hayashi, D.S. Sutherland, H. Autrup, Toxicity of silver nanoparticles-nanoparticle or silver ion? Toxicol. Lett. 208 (2012) 286–292, https://doi.org/10.1016/j.toxlet.2011.11.002.

[25] Y.S. Kim, M.Y. Song, J.D. Park, K.S. Song, H.R. Ryu, Y.H. Chung, H.K. Chang, J. H. Lee, K.H. Oh, B.J. Kelman, I.K. Hwang, I.J. Yu, Subchronic oral toxicity of silver nanoparticles, Part. Fibre Toxicol. 7 (2010) 1–11, https://doi.org/10.1186/1743-8977-7-20.

[26] A.D. Permana, M. Mir, E. Utomo, R.F. Donnelly, Bacterially sensitive nanoparticle-based dissolving microneedles of doxycycline for enhanced treatment of bacterial biofilm skin infection: a proof of concept study, Int. J. Pharm. X. 2 (2020) 100047, https://doi.org/10.1016/j.ijpx.2020.100047.

[27] M.H. Xiang, Y. Bao, X.Z. Yang, Y.C. Wang, B. Sun, J. Wang, Lipase-sensitive polymeric triple-layered nanogel for "on-demand" drug delivery, J. Am. Chem. Soc. 134 (2012) 4355–4362.

[28] C. Han, N. Romero, S. Fischer, J. Dookran, A. Berger, A.L. Doiron, Recent developments in the use of nanoparticles for treatment of biofilms, Nanotechnol. Rev. 6 (2017) 383–404.

[29] M. Lengyel, N. Kállai-Szabó, V. Antal, A.J. Laki, I. Antal, Microparticles, microspheres, and microcapsules for advanced drug delivery, Sci. Pharm. 87 (2019). doi:https://doi.org/10.3390/scipharm87030020.

[30] S.P. Noel, H.S. Courtney, J.D. Bumgardner, W.O. Haggard, Chitosan sponges to locally deliver amikacin and vancomycin: a pilot in vitro evaluation, Clin. Orthop. Relat. Res. 468 (2010) 2074–2080.

[31] E. Caffarel-Salvador, M.C. Kearney, R. Mairs, L. Gallo, S.A. Stewart, A.J. Brady, R. F. Donnelly, Methylene blue-loaded dissolving microneedles: potential use in photodynamic antimicrobial chemotherapy of infected wounds, Pharmaceutics. 7 (2015) 397–412.

[32] S.V. Bharambe, A.B. Darekar, R.B. Saudagar, Wound healing dressings and drug delivery systems: a review, Int. J. Pharm. Technol. 5 (2013) 2764–2786.

[33] B.A. Lipsky, C. Hoey, Topical antimicrobial therapy for treating chronic wounds, Clin. Infect. Dis. 49 (2009) 1541–1549.

[34] A.D. Permana, M.T.C. McCrudden, R.F. Donnelly, Enhanced intradermal delivery of nanosuspensions of antifilariasis drugs using dissolving microneedles: a proof of concept study, Pharmaceutics. 11 (2019) 346.

[35] A.J. Paredes, P.E. McKenna, I.K. Ramöller, Y.A. Naser, F. Volpe-Zanutto, M. Li, M. T.A. Abbate, L. Zhao, C. Zhang, J.M. Abu-Ershaid, X. Dai, R.F. Donnelly, Microarray patches: poking a hole in the challenges faced when delivering poorly soluble drugs, Adv. Funct. Mater. 2005792 (2020) 1–27, https://doi.org/10.1002/adfm.202005792.

[36] A.D. Permana, I.A. Tekko, M.T.C. McCrudden, Q.K. Anjani, D. Ramadon, H. O. McCarthy, R.F. Donnelly, Solid lipid nanoparticle-based dissolving microneedles: a promising intradermal lymph targeting drug delivery system with potential for enhanced treatment of lymphatic filariasis, J. Control. Release 316 (2019) 34–52.

[37] S. Sartini, M.N. Djide, M.N. Amir, A.D. Permana, Phenolic-rich green tea extract increases the antibacterial activity of amoxicillin against *Staphylococcus aureus* by in vitro and ex vivo studies, 8 (2020) 491–500.

[38] J.B. Patel, R.F. Cockerill, A.P. Bradford, M.G. Eliopoulos, A.J. Hindler, G.S. Jenkins, S.J. Lewis, B. Limbago, A.L. Miller, P.D. Nicolau, P.. M., M.J. Swenson, M. M. Traczewski, J.D. Turnidge, P.M. Weinstein, L.B. Zimmer, Methods for dilution antimicrobial susceptibility tests for bacteria that grow aerobically; Approved Standard—Tenth Edition., CLSI (Clinical Lab. Stand. Institute). 35 (2015).

[39] H. Chen, L. Li, Y. Liu, M. Wu, S. Xu, G. Zhang, C. Qi, Y. Du, M. Wang, J. Li, X. Huang, In vitro activity and post-antibiotic effects of linezolid in combination with fosfomycin against clinical isolates of Staphylococcus aureus, Infect. Drug Resist. 11 (2018) 2107–2115.

[40] A.D. Permana, A.J. Paredes, F. Volpe-Zanutto, Q.K. Anjani, E. Utomo, R. F. Donnelly, Dissolving microneedle-mediated dermal delivery of itraconazole nanocrystals for improved treatment of cutaneous candidiasis, Eur. J. Pharm. Biopharm. 154 (2020) 50–61, https://doi.org/10.1016/j.ejpb.2020.06.025.

[41] M.M. Bazargani, J. Rohloff, Antibiofilm activity of essential oils and plant extracts against Staphylococcus aureus and Escherichia coli biofilms, Food Control 61 (2016) 156–164.

[42] J. Godbee, E. Scott, P. Pattamunuch, S. Chen, E. Mathiowitz, Role of solvent/non-solvent ratio on microsphere formation using the solvent removal method, J. Microencapsul. 21 (2004) 151–160, https://doi.org/10.1080/02652040310001637875.

[43] P. González-Vázquez, E. Larrañeta, M.T.C. McCrudden, C. Jarrahian, A. Rein-Weston, M. Quintanar-Solares, D. Zehrung, H. McCarthy, A.J. Courtenay, R. F. Donnelly, Transdermal delivery of gentamicin using dissolving microneedle arrays for potential treatment of neonatal sepsis, J. Control. Release 265 (2017) 30–40.

[44] E. Larrañeta, J. Moore, E.M. Vicente-Pérez, P. González-Vázquez, R. Lutton, A. D. Woolfson, R.F. Donnelly, A proposed model membrane and test method for microneedle insertion studies, Int. J. Pharm. 472 (2014) 65–73, https://doi.org/10.1016/j.ijpharm.2014.05.042.

[45] Y. Zhang, M. Huo, J. Zhou, S. Xie, PKSolver: an add-in program for pharmacokinetic and pharmacodynamic data analysis in Microsoft excel, Comput. Methods Prog. Biomed. 99 (2010) 306–314.

[46] E.D. Roche, E.J. Woodmansey, Q. Yang, D.J. Gibson, H. Zhang, G.S. Schultz, Cadexomer iodine effectively reduces bacterial biofilm in porcine wounds ex vivo and in vivo, Int. Wound J. 16 (2019) 674–683.

[47] P. Singh, Y.J. Kim, D. Zhang, D.C. Yang, Biological synthesis of nanoparticles from plants and microorganisms, Trends Biotechnol. 34 (2016) 588–599, https://doi.org/10.1016/j.tibtech.2016.02.006.

[48] C. Tamuly, M. Hazarika, S.C. Borah, M.R. Das, M.P. Boruah, In situ biosynthesis of Ag, Au and bimetallic nanoparticles using Piper pedicellatum C.DC: Green chemistry approach, Colloids Surfaces B Biointerfaces. 102 (2013) 627–634.

[49] B.S. de O. Silva, A.B. Seabra, Characterization of iron nanoparticles produced with green tea extract: a promising material for nitric oxide delivery, Biointerface Res. Appl. Chem. 6 (2016).

[50] A. Dutt, L.S.B. Upadhyay, Synthesis of cysteine-functionalized silver nanoparticles using green tea extract with application for lipase immobilization, Anal. Lett. 51 (2018) 1071–1086, https://doi.org/10.1080/00032719.2017.1367399.

[51] A. Saxena, R.M. Tripathi, F. Zafar, P. Singh, Green synthesis of silver nanoparticles using aqueous solution of Ficus benghalensis leaf extract and characterization of their antibacterial activity, Mater. Lett. 67 (2012) 91–94, https://doi.org/10.1016/j.matlet.2011.09.038.

[52] Q. Sun, X. Cai, J. Li, M. Zheng, Z. Chen, C.P. Yu, Green synthesis of silver nanoparticles using tea leaf extract and evaluation of their stability and antibacterial activity, Colloids Surfaces A Physicochem. Eng. Asp. 444 (2014) 226–231.

[53] A.B. Seabra, N. Manosalva, B. De Araujo Lima, M.T. Pelegrino, M. Brocchi, O. Rubilar, N. Duran, Antibacterial activity of nitric oxide releasing silver nanoparticles, J. Phys. Conf. Ser. 838 (2017). doi:https://doi.org/10.1088/1742-6596/838/1/012031.
[54] M.A. Mumuni, F.C. Kenechukwu, O.C. Ernest, A.M. Oluseun, B. Abdulmumin, D. C. Youngson, O.C. Kenneth, A.A. Anthony, Surface-modified mucoadhesive microparticles as a controlled release system for oral delivery of insulin, Heliyon. 5 (2019), e02366, https://doi.org/10.1016/j.heliyon.2019.e02366.
[55] Y. yu Ren, H. Yang, T. Wang, C. Wang, Green synthesis and antimicrobial activity of monodisperse silver nanoparticles synthesized using *Ginkgo biloba* leaf extract, Phys. Lett. Sect. A Gen. At. Solid State Phys. 380 (2016) 3773–3777. doi:https://doi.org/10.1016/j.physleta.2016.09.029.
[56] M. Tato, Y. López, M.I. Morosini, A. Moreno-Bofarull, F. Garcia-Alonso, D. Gargallo-Viola, J. Vila, R. Cantón, Characterization of variables that may influence ozenoxacin in susceptibility testing, including MIC and MBC values, Diagn. Microbiol. Infect. Dis. 78 (2014) 263–267.
[57] N. Durán, M. Durán, M.B. de Jesus, A.B. Seabra, W.J. Fávaro, G. Nakazato, Silver nanoparticles: a new view on mechanistic aspects on antimicrobial activity, nanomedicine nanotechnology, Biol. Med. 12 (2016) 789–799, https://doi.org/10.1016/j.nano.2015.11.016.
[58] N. Høiby, T. Bjarnsholt, M. Givskov, S. Molin, O. Ciofu, Antibiotic resistance of bacterial biofilms, Int. J. Antimicrob. Agents 35 (2010) 322–332.
[59] J.N. Anderl, M.J. Franklin, P.S. Stewart, Role of antibiotic penetration limitation in Klebsiella pneumoniae biofilm resistance to ampicillin and ciprofloxacin, Antimicrob. Agents Chemother. 44 (2000) 1818–1824.
[60] J.P. Folsom, B. Baker, P.S. Stewart, In vitro efficacy of bismuth thiols against biofilms formed by bacteria isolated from human chronic wounds, J. Appl. Microbiol. 111 (2011) 989–996.
[61] E.I. Rabea, M.E.T. Badawy, C.V. Stevens, G. Smagghe, W. Steurbaut, Chitosan as antimicrobial agent: applications and mode of action, Biomacromolecules. 4 (2003) 1457–1465.
[62] M. Mir, N. Ahmed, A.D. Permana, A.M. Rodgers, R.F. Donnelly, A.U. Rehman, Enhancement in site-specific delivery of carvacrol against methicillin resistant staphylococcus aureus induced skin infections using enzyme responsive nanoparticles: a proof of concept study, Pharmaceutics. 11 (2019) 606.
[63] S.H. Chiou, W.T. Wu, Immobilization of Candida rugosa lipase on chitosan with activation of the hydroxyl groups, Biomaterials. 25 (2004) 197–204.
[64] J. Park, M.G. Allen, M.R. Prausnitz, Polymer microneedles for controlled-release drug delivery, Pharm. Res. 23 (2006) 1008–1019.
[65] B. Pamornpathomkul, T. Ngawhirunpat, I.A. Tekko, L. Vora, H.O. McCarthy, R. F. Donnelly, Dissolving polymeric microneedle arrays for enhanced site-specific acyclovir delivery, Eur. J. Pharm. Sci. 121 (2018) 200–209, https://doi.org/10.1016/j.ejps.2018.05.009.
[66] L.K. Vora, P.R. Vavia, E. Larrañeta, S.E.J. Bell, R.F. Donnelly, Novel nanosuspension-based dissolving microneedle arrays for transdermal delivery of a hydrophobic drug, J. Interdiscip. Nanomedicine. 3 (2018) 89–101.
[67] M.T.C. McCrudden, A.Z. Alkilani, C.M. McCrudden, E. McAlister, H.O. McCarthy, A.D. Woolfson, R.F. Donnelly, Design and physicochemical characterisation of novel dissolving polymeric microneedle arrays for transdermal delivery of high dose, low molecular weight drugs, J. Control. Release 180 (2014) 71–80.
[68] R.F. Donnelly, K. Moffat, A.Z. Alkilani, E.M. Vicente-Pérez, J. Barry, M.T. C. McCrudden, A.D. Woolfson, Hydrogel-forming microneedle arrays can be effectively inserted in skin by self-application: a pilot study centred on pharmacist intervention and a patient information leaflet, Pharm. Res. 31 (2014) 1989–1999.
[69] R.F. Donnelly, M.J. Garland, D.I.J. Morrow, K. Migalska, T. Raghu, R. Singh, R. Majithiya, A.D. Woolfson, Optical coherence tomography is a valuable tool in the study of the effects of microneedle geometry on skin penetration characteristics and in-skin dissolution, J. Control. Release 147 (2010) 333–341.
[70] R.E.M. Lutton, E. Larrañeta, M.C. Kearney, P. Boyd, A.D. Woolfson, R.F. Donnelly, A novel scalable manufacturing process for the production of hydrogel-forming microneedle arrays, Int. J. Pharm. 494 (2015) 417–429.
[71] M. Mir, N. Ahmed, A.D. Permana, A.M. Rodgers, R.F. Donnelly, A.U. Rehman, Enhancement in site-specific delivery of carvacrol against methicillin resistant *Staphylococcus aureus* induced skin infections using enzyme responsive nanoparticles: A proof of concept study, Pharmaceutics. 11 (2019). doi:https://doi.org/10.3390/pharmaceutics11110606.